Revised draft of 2009 December 7

OB Stars & Stellar Bowshocks in Cygnus-X: A Novel Laboratory Estimating Stellar Mass Loss Rates

Henry A. Kobulnicky

Department of Physics & Astronomy
1000 E. University
University of Wyoming
Laramie, WY 82071
Electronic Mail: chipk@uwyo.edu

Ian J. Gilbert[1]

Department of Physics
100 Campus Drive
Grove City College
Grove City, PA 16127
Electronic Mail: gilbertij1@gcc.edu

Daniel C. Kiminki

Department of Physics & Astronomy
1000 E. University
University of Wyoming
Laramie, WY 82070
Electronic Mail: kiminki@uwyo.edu

ABSTRACT

We use mid-IR images from the *Spitzer Space Telescope* Cygnus X Legacy Survey to search for stellar bowshocks, a signature of early type "runaway" stars

---

[1]Also at Department of Physics & Astronomy
1000 E. University
University of Wyoming
Laramie, WY 82070

with high space velocities. We identify ten arc-shaped nebulae containing centrally located stars as candidate bowshocks. New spectroscopic observations of five stars show that all are late O to early B dwarfs, while one is a previously classified B0.2 giant. These stars have moderate radial velocities, differing by ΔV <10 km s^{-1} from members of the Cygnus OB2 Association. The spectral energy distributions of the other four stars are consistent with late O to early B dwarfs at the nominal ∼1.6 kpc distance of Cyg OB2. Our morphologically selected sample of bowshock candidates encompasses diverse physical phenomena. Three of the stars appear to be pre-main-sequence objects on the basis of rising SEDs in the mid-IR, and their nebulae may be photon-dominated regions (PDRs) illuminated by the central star but shaped by external sources such as winds from Cyg OB2. Four objects have ambiguous classification. These may be partial dust shells or bubbles. We conclude that three of the objects are probable bowshocks, based on their morphological similarity to analytic prescriptions. Their nebular morphologies reveal no systematic pattern of orientations that might indicate either a population of stars ejected from or large-scale hydrodynamic outflows from Cyg OB2. The fraction of runaways among OB stars near Cyg OB2 identified either by radial velocity or bowshock techniques is ∼0.5%, much smaller than the ∼8% estimated among field OB stars. We discuss possible reasons for this difference. We also obtained a heliocentric radial velocity for the previously known bowshock star, BD+43°3654, of -66.2 ± 9.4 km s^{-1}, solidifying its runaway status and implying a space velocity of 77±10 km s^{-1}. We use the principles of momentum-driven bowshocks in conjunction with the observed sizes, bowshock luminosities & spectral energy distributions, and dust/PAH emission models to arrive at a novel method for estimating stellar mass loss rates. Derived mass loss rates range between 10^{-7} and few$\times10^{-6}$ M$_\odot$ yr^{-1} for the three O5V – ∼B2V stars identified as generating bowshocks. These values are at the upper range of, but broadly consistent with, estimates from other methods. We calculate a relatively large mass loss rate of 160×10^{-6} M$_\odot$ yr^{-1} for O4If star BD+43°3654 using the same method.

Subject headings: stars: early-type – stars: individual: BD+43°3654, HD 195229, GSC 03161-01188–Galaxy: open clusters and associations: individual: Cygnus OB2

1. Introduction

Most OB stars lie within the associations in which they were born. However, a significant fraction (17%–50%) having high (30–200 km s^{-1}) space velocities wander far from such associations and are known as "runaways" (Blaauw 1961; Stone 1982; Conti et al. 1977; Gies & Bolton 1986). Often, these stars' proper motions allow them to be traced back to a known OB association in which they presumably formed. The speed necessary for a star to be classified as a runaway varies from 30–40 km s^{-1} depending on author. We adopt the 30 km s^{-1} criterion used by Gies & Bolton (1986).

Blaauw (1961) suggested that runaway stars are ejected from OB associations when one member of a binary system sheds a large fraction of its mass, as in a type II supernova. In this case (known as the binary-supernova scenario), the surviving companion is released with a velocity comparable to its previous orbital velocity. Blaauw (1961) cited the low binary frequency of runaway stars as evidence for this model, though Gies & Bolton (1986) found a few runaway binaries in their survey. Whether and how frequently supernovae in binary systems produce an unbound, high-velocity O star is an active line of investigation.

Gies & Bolton (1986) proposed that runaway stars are ejected during close encounters between binary systems in OB associations. This model, known as the dynamical-ejection scenario, explains the existence of binary runaway systems, since hard encounters among three or more stars can produce both single runaway stars and binary runaway systems. Leonard & Duncan (1988, 1990) performed numerical simulations of young star clusters, showing that dynamical encounters can readily account for the number of observed runaways and that runaway binary systems are possible.

Hoogerwerf, de Bruijne, & de Zeeuw (2000) used precision proper-motion measurements of nearby runaways to find evidence for both binary-supernova and dynamical ejection mechanisms. They concluded that the runaway ζ Oph likely resulted from the dissociation of a binary system wherein the other member became the pulsar PSR J1932+1059. They also concluded that the runaways AE Aurigae and μ Columbae and the binary system ι Orionis were produced in a binary-binary encounter.

Traditionally, runaway stars reveal themselves through their high proper motions or unusually large radial velocities (Gies & Bolton 1986; Mdzinarishvili & Chargeishvili 2005). Identification using radial velocities requires high-precision spectra, and this technique is sensitive only to runaways with large projected radial velocity components. Identification on the basis of high proper motions requires precise astrometric data, such as those made by the Hipparcos (Perryman et al. 1997) mission, along with secure distance measurements. This technique is only sensitive to runaways with large tangential motions.

Runaway O stars have also been identified by detecting the tell-tale "bowshocks" produced when the stellar winds of stars traveling supersonically impinge upon the surrounding interstellar medium. Bowshocks appear as symmetric arc-shaped features with apsides oriented in the direction of the stars' motions and at distances from the star determined by momentum balance between the wind and the ambient medium. van Buren & McCray (1988), van Buren et al. (1995), and Noriega-Crespo et al. (1997) used Infrared Astronomical Satellite (IRAS) images to locate arc-shaped features associated with high-velocity O stars. These studies noted that a variety of phenomena can produce bowshock-like morphologies, including partial stellar wind bubbles and dust shells, H II regions with density gradients, and genuine high-velocity stars. Indeed, we conclude that our sample is comprised of a mixture of such objects. Several more recent studies have used Hα surveys, Midcourse Space Experiment (MSX) and *Spitzer Space Telescope (SST)* infrared images to detect bowshocks and associate them with high-velocity O stars (Brown & Bomans 2005; Comerón & Pasquali 2007; Gvaramadze & Bomans 2008; Povich et al. 2008). Bowshocks are also seen in environments such as the Orion Nebula where winds and jets from young encounter the O-star winds that power the nebula (e.g., the *HST* images of Bally et al. (2000)).

In this paper we use infrared images from the *SST* Cygnus-X Legacy Survey (Hora et al. 2007) to identify bowshock candidates in the vicinity of one of the Galaxy's richest OB associations. The association Cygnus OB2, at the heart of the Cygnus X region, contains over 100 OB stars, including an O3If and O4If (Massey & Thompson 1991; Hanson 2003; Comerón et al. 2002; Comerón & Pasquali 2007). The spectroscopic OB survey of 142 stars in Cygnus OB2 by Kiminki et al. (2007) did not detect any runaway stars on the basis of radial velocities. However, in a region as rich in young massive stars as Cygnus OB2, one would also expect to find stars ejected with large motions in the plane of the sky. Comerón & Pasquali (2007) implicate Cygnus OB2 as the origin of one such star, the O4If runaway BD+43°3654, using the morphology of the bowshock seen in *MSX* images. Given the superior sensitivity and angular resolution of *SST*, a more complete search may now be conducted for runaway stars hosting bowshocks in this region. Herein, we describe the discovery of ten candidate bowshocks near Cygnus OB2, and we report followup optical spectroscopy that allows us to determine the spectral types and radial velocities for a subset of the central stars that power each candidate. We refer to the bowshock candidates and their central stars separately as Bowshocks (BS) 1–10 and Stars 1–10. We also investigate a novel method of determining the mass loss rates of these stars using the principles of momentum-driven bowshocks.

Modern distance estimates to Cyg OB2 range from 1.7 kpc (Massey & Thompson 1991; Torres-Dodgen et al. 1991) to 1.4 kpc (Hanson 2003). We adopt d=1.6 kpc, at which distance 1 pc corresponds to 130$''$ on the sky.

2. Data

2.1. Spitzer Space Telescope

We retrieved data from the *SST* archive obtained as part of the *Spitzer* Legacy Survey of the Cygnus-X Complex (Hora et al. 2007) using data from the Infrared Array Camera (IRAC) at 3.6, 4.5, 5.8, and 8.0 microns (Fazio et al. 2004) and the Multi-band Infrared Photometer for Spitzer (MIPS) bandpasses at 24 & 70 microns (Rieke et al. 2004). One of us (HAK) visually examined mosaiced single-band and multi-color images of the $\sim$24 square degree survey area to identify bowshock candidates on the basis of symmetric arc-shaped structures less than a few arcminutes in size enclosing a symmetrically placed stellar source. The complex ISM structure in this region, coupled with the large dynamic range of features, renders bowshock identification a subjective and imprecise task. In practice, the 8-micron band (sensitive to emission from PAH features excited by non-ionizing photons) and the 24-micron band (sensitive to emission from warm dust) were the principal images used to locate candidate bowshocks. While a plethora of arc-like structures appear in both bands, very few exhibited a high degree of symmetry and included a point source near the apsis. In total, ten objects were deemed to be bowshock candidates and were retained for further investigation. Table 1 lists the equatorial & Galactic coordinates and 2MASS JHK & *SST* IRAC photometry of the central stars for each object. The final column provides common stellar cross identifications from other works, where applicable.

Figure 1 is a 3-color image $\sim 2°$ square centered on Cygnus OB2 ($\ell = 80.3°$, $b = +1.0°$) showing the location of the first seven candidate bowshocks. Blue, green, and red represent the 4.5, 8.0, and 24 micron images, respectively. Objects 8–10 have Galactic latitudes $b < 0.15°$ and lie off the lower edge of Figure 1. Figures 2 through 11 show enlarged views of each bowshock candidate using the same color scheme as Figure 1. We discuss each object in detail in §3.

2.2. WIRO

We obtained optical spectra for several of the stellar sources located near the apsides of candidate bowshocks. We observed five of the stars (Stars 1, 2, 3, 5, and 8) at the Wyoming Infrared Observatory's (WIRO) 2.3 m telescope equipped with the Longslit spectrograph on 2008 June 23–30, 2009 May 20, and 2009 September 16. The 1800 l mm^{-1} grating was used in first order. The spectral coverage was 5210–6680 Å. Exposure time varied from 360 s for Star 3 (HD 195229) to 3600 s for Stars 2 and 5, yielding signal-to-noise ratios ranging from 50:1 for Star 5 to 450:1 for Star 2. Copper-Argon lamp exposures were taken after each stellar spectrum for wavelength calibration.

The spectra were reduced, extracted, wavelength calibrated, and Doppler corrected to the heliocentric frame using standard IRAF[1] tasks in the KPNOSLIT package. The absolute radial velocities were checked against the standards HD161096, HD 161797, HD131156, HD171391, and HD188512. Table 1 lists the heliocentric radial velocities, which are typically accurate to 6 km s^{-1} rms.

2.3. WIYN

We also obtained spectra of BD+43°3654 and HD195229 during an observing run at the WIYN[2] 3.5 m telescope on 2008 June 11–16 using the Hydra multispectrograph. We used the Red camera and 3″ blue fiber cables with the 1200 l mm^{-1} grating in second order. Exposure times were 600 s and the spectral coverage was 3820–4500 Å. Copper-Argon lamp exposures were taken to wavelength calibrate the spectra. The spectra were reduced, extracted, wavelength calibrated, and Doppler corrected to the heliocentric frame using standard IRAF tasks in the TWODSPEC and RVCOR packages. Radial velocities of standards HD 131156, HD146233, HD161096, HD161797, and HD171391 from this run agreed with published values to ±2 km s^{-1}.

3. Analysis

3.1. Bowshock Identification and Images

Figure 1 shows a portion of the Cygnus-X region surrounding its most massive and energetic constituent, Cygnus OB2. This region encompasses a complex array of nebulae and star-forming regions located at various distances along the line of sight, with most of the activity located in the local or "Orion" spiral arm at a distance of 1–2 kpc. Odenwald & Schwartz (1993) present a schematic 3-dimensional representation of the Cygnus-X region, while Schneider et al. (2006) provide velocity-resolved molecular maps of Cygnus-X and individual star-forming objects nearby. One apparent feature of this region is the relative

---

[1]IRAF is distributed by the National Optical Astronomy Observatories, which are operated by the Association of Universities for Research in Astronomy, Inc., under cooperative agreement with the National Science Foundation.

[2]The WIYN Observatory is a joint facility of the University of Wisconsin-Madison, Indiana University, Yale University, and the National Optical Astronomy Observatories.

absence of dust (red) and PAH emission (green) at the location of Cyg OB2 itself, except at the southern edge. This apparent "hole" is consistent with a cavity cleared by the winds of >100 evolving massive stars. Some of the prominent star-forming regions labeled in Figure 1 clearly constitute the heads of gaseous pillars, most of which point toward Cyg OB2, the dominant source of luminous and mechanical energy in this vicinity. These pillars are reminiscent of those in M 16 (Indebetouw et al. 2007; Hester et al. 1996), RCS 49 (Whitney et al. 2004) and other massive star-forming regions.

The seven bowshock candidates labeled in Figure 1 lie around the periphery of Cyg OB2, none falling within the main concentration of Cyg OB2 stars but all within ∼5–8 pc of the canonical Cyg OB2 center. The orientations of the features, seen more clearly in Figures 2 through 11, appear random, having no preferential alignment with respect to Cyg OB2. Generically, bowshock orientation reveals the relative motion between the star and surrounding matter. We might have expected, if the stars were all runaways from Cyg OB2, that the bowshocks would point away from the Association in the direction of the stars' motions. On the other hand, if the hydrodynamics of material surrounding Cyg OB2 were dominated by a hot outflow from an over-pressured region, we might have expected many of the bowshocks to point back toward the source of mechanical energy, as do three bowshocks near M 17 and at least one near RCW 49 (Povich et al. 2008). The absence of either signature suggests that 1) the central stars driving the bowshocks, if they are runaways, have different origins, and 2) there is no large-scale supersonic wind emanating from Cyg OB2. Only candidates 2 and 4 have orientations consistent with their stars being runaways having an origin within Cyg OB2.

3.2. Nebular and Stellar SEDs

The colors of the candidate bowshock nebulae , best seen in the individual zoomed images in Figures 2 through 11, at first glance reveal two classes of objects. Candidates 1,3,4,7 are seen exclusively at 24 microns and longer wavelengths while the rest exhibit strong emission in the IRAC bandpasses with some additional contribution at longer wavelengths.

We performed aperture photometry of each bowshock candidate in each of the six bandpasses using the *SSC* post-basic calibrated data mosaic images by assigning irregular crescent-shaped polygonal apertures defined visually on the [8.0] and/or [24] images. We also manually defined background regions surrounding each bowshock. Because these objects lie in complex regions of diffuse emission, care was taken to select multiple background regions judged to be representative of the local background away from the nebula but within several arcminutes. We applied aperture corrections, as recommended in the IRAC and MIPS calibration web pages[3], using values appropriate to a circular aperture of equivalent area to the polygonal apertures. These corrections are less than 1.3 in all cases and are sometimes less than unity for the IRAC bands. Given the imprecision of the aperture corrections and the high and variable background levels, we adopt a minimum uncertainty of 20% in all bands. Table 2 gives background-subtracted aperture fluxes in mJy for all of the nebulae. In some cases, only 1σ upper limits are given, mostly in the IRAC bands where some objects are not detected.

For each bowshock candidate we were able to identify a symmetrically placed point source, presumed to be the energizing star, behind the apsis. Figure 12 is a 2MASS JHK color-color diagram showing each of the ten stars (*diamonds*) associated with the bowshocks. The solid and dashed curves (*asterisks and crosses, respectively*) show a fiducial main sequence and supergiant sequence. A solid line illustrates the reddening vector for $A_V = 5$ mag. The majority of stars lie in a close group near H-K=0.3, J-H=0.6, consistent with early-type stars seen behind 4–7 magnitudes of visual extinction. This range is similar to other OB stars in Cyg OB2 (Massey & Thompson 1991), suggesting that they lie at a similar distance. Stars 4 and 6 are much redder, suggesting 12–15 magnitudes of visual extinction, under the assumption that these are also early-type stars. The K-band magnitudes for these two stars are 2–3 magnitudes fainter than the other targets, indicating either a larger distance or the effect of localized regions of high extinction. Star 6, in particular, is surrounded by a more substantial region of warm dust and photo-excited material, consistent with localized extinction. Star 3 (HD195229), a known B0.2III, is much less red, consistent with $\sim$1 magnitude of visual extinction, and consistent with the known variability of extinction across Cyg OB2 (Massey & Thompson 1991).

We performed aperture photometry on the central star of each bowshock at the mid-IR IRAC bandpasses using the *SSC* basic calibrated data frames, a 10-pixel circular aperture for which the aperture correction is minimal, and a much larger annulus to measure the diffuse background levels. Most of the stars were saturated at IRAC [3.6] and [4.5] bands in the 10.4 s exposures, so the high-dynamic-range (HDR) 0.4 s exposures were used. Table 1 lists these fluxes and their uncertainties.

Figure 13 shows the spectral energy distributions of the bowshock candidates and central stars at the 2MASS, IRAC and two MIPS bandpasses. Asterisks denote photometry of the bowshock alone, while diamonds denote the star plus bowshock. The bowshocks are not detected at 2MASS JHK bands and are somtimes undetected in the IRAC bandpasses. In only three cases (stars 6, 8, and 9) are pointlike sources detected at [24], indicative of dust

[3]http://ssc.spitzer.caltech.edu/irac/calib/ ; http://ssc.spitzer.caltech.edu/mips

in the immediate vicinity of the stars. Uncertainties are always smaller than the plotted points. The solid curves are blackbody fits to the JHK photometry, while the dotted curves are fits to the IRAC and MIPS data using scaled Draine & Li (2007) dust emission models. In Sections 3.4 and 4 we discuss the details of the fitting, the models, and model results for each object individually.

3.3. Bowshock Candidate Morphologies

The shape of a momentum-driven bowshock is a universal function that scales as the "standoff distance", R_0, between the star and the bowshock apsis, as shown analytically by Baranov et al. (1971); Dyson (1975); van Buren et al. (1990); Wilkin (1996). Using the formulation of Wilkin (1996) Equation 9, we generated synthetic bowshock "images", applying arbitrary size, rotation, and intensity scale factors to facilitate comparison with the data. Figure 14 shows a selected subset of bowshock candidates (1, 2, 3, 5, 6, and 7) at [8.0] (*green*), [24] (*red*) and the scaled synthetic bowshock (*blue*). The simulated bowshocks are all shown at zero degrees inclination, while the inclinations of the bowshock candidates are unknown.

The morphologies of candidates 5 and 7 (central stars O9V and O5V) show striking similarity to the theoretical shape. The agreement is best at [24] where the bowshock can be traced to larger radial distances than at [8.0] where the bowshock is less extended and exhibits a more irregular morphology. For object 2, there is also good agreement, although the bowshock itself is faint and difficult to see because of the large dynamic range in the images. For objects 1, 3, and 6 the morphological agreement is considerably less good. We take this as evidence for a physical origin other than a bowshock. The morphologies of the other objects 4, 8, 9, and 10 (not pictured) also differ from the canonical bowshock shape, appearing more irregular and clumpy. We interpret the good agreement between the model shape and objects 2, 5, and 7 as support for the momentum-driven bowshock nature of these objects.

3.4. Individual Objects

3.4.1. Bowshock Candidate 1 and Star 1 (GSC03161-01188)

Bowshock candidate 1, pictured in Figure 2, is associated with the V=13.3 star GSC03161-01188 from the Guide Star Catalog, also known as #1288 from the work of Reddish et al. (1966). Figure 15 (bottom) shows the WIRO spectrum of GSC03161-01188. We classify

GSC03161-01188 as O9V on the basis of the HeI/HeII line ratios and by comparison to a Jacoby et al. (1984) spectral library O9V star (top). We compute a spectrophotometric distance for the K=8.21 star GSC03161-01188 by adopting a visual extinction of 4.5 magnitudes from Figure 12 ($A_K = 0.51$ mag), an intrinsic color V-K=−0.85, and assuming an absolute magnitude for an O9V star of $M_V = 4.05 \pm 0.2$ (Martins et al. 2005). This yields a spectrophotometric distance of 1500 ± 150 pc for GSC03161-01188, consistent with the adopted distance to Cyg OB2, ∼ 1.6 kpc (Hanson 2003; Massey & Thompson 1991; Schulte 1958).

Cross correlating the spectrum of GSC03161-01188 with a synthetic model atmosphere O9V spectrum from Lanz & Hubeny (2003), as described more fully in Kiminki et al. (2007), yields a heliocentric radial velocity of -17 ± 6 km s^{-1}. This velocity is consistent with, but more negative than, the average radial velocities of Cyg OB2 members, -10 ± 6 km s^{-1} surveyed by Kiminki et al. (2007).

The spectral energy distribution in Figure 13 shows that this nebula is detected only at [24] and [70]. Stellar flux dominates the 2MASS and IRAC bandpasses. The solid line shows the SED of an O9.5V star, approximated as a blackbody with T_{eff}=30,000 K and R=8 $R_{\odot}$, (Martins et al. 2005) which, at a distance of 1.6 kpc with $A_V = 4.5$ mag, provides a good fit to the near-IR data. This is consistent with our spectral classification based on Figure 15.

Given the lack of similarity to the theoretical shape and the modest radial velocity of the central star, this nebula is unlikely to be a bowshock. We assign this object an ambiguous classification. Possibilities include a dusty asymmetric bubble or a partial shell.

3.4.2. Bowshock Candidate 2 and Star 2 (G80.9020+0.9828)

Figure 2 shows bowshock candidate 2 and Star 2 (G80.9020+0.9828). Figure 16 (bottom) shows the WIRO spectrum of this star and a comparison B2 dwarf equivalent from the model atmospheres of Lanz & Hubeny (2003) (top). The relative strengths of the H I 6563 Å and the He I 6678 Å and He I 5876 Å lines lead us to classify this star as B2V, plus or minus several spectral subtypes, owing to the low signal-to-noise spectrum. Its heliocentric radial velocity is -12 ± 15 km s^{-1}, consistent with the range of radial velocities observed for Cyg OB2 members Kiminki et al. (2007). We compute a spectrophotometric distance from the 2MASS photometry (K=10.5) by adopting a visual extinction (Cardelli et al. 1989) of 4.5 magnitudes ($A_K = 0.51$), an absolute magnitude for an B2V star of $M_V = -2.4 \pm 0.4$, an intrinsic V-K color of -0.4. This yields a spectrophotometric distance of 2500 ± 500 pc, where the error is driven primarily by the uncertainty on the spectral type/absolute magnitude.

A high-surface-brightness apsis lies 9″ (0.07 pc projected separation) from the star toward the upper left in Figure 2, and there is also a more extended region of 8 micron emission preceding the apsis to the upper left. The [24] lima-bean shaped nebulosity and the arc-like structure seen at [8.0] do not share a common symmetry axis, so it is difficult to ascertain which wavelength best traces the putative bowshock.

Figure 13 shows that Bowshock 2 is a strong detection at the IRAC and MIPS bandpasses. The relative faintness of the bowshock in [4.5] relative to the other three IRAC bandpasses is consistent with strong PAH emission in the shock. The central star dominates the 2MASS bandpasses. Star 2 is fainter than Star 1, and is well fit by a B2V–B3V star (T_{eff}=20,000 K, R=4 $R_{\odot}$) at a distance of 1.6 kpc with an extinction of $A_V = 4.5$ mag (*solid line*).

Although this candidate bowshock nebula is faint and difficult to represent owing to a large dynamic range in the images, the morphological agreement with the theoretical shape is reasonably good. The apsis of this nebula is bright at [8.0] and [24] and may indicate an interaction or illumination of a of a nearby cloud. We retain this object as a probable showshock.

3.4.3. Bowshock Candidate 3 and Star 3 (HD195229)

Bowshock candidate 3 appears to be generated by its attendant star, HD195229, listed as B0.2III in SIMBAD. Figures 17 and 18 show our WIRO and WIYN spectra of this star, from which we confirm a B0.2III spectral type. From these spectra we find a heliocentric radial velocity of -3 ± 2 km s^{-1}, slightly less negative than other massive stars near Cyg OB2. The luminosity for a B0.2 giant is somewhat uncertain because the evolutionary tracks for massive giant and supergiant stars are nearly vertical in an H-R diagram (Marigo et al. 2008). Assuming $M_V = -5 \pm 0.5$, V-K=-0.8 and $A_V = 1.0$ from Figure 12 for this $K = 7.3$ star leads to a spectrophotometric distance of 1800 ± 500 pc, consistent with the distances of massive stars in Cyg OB2.

HD195229 is also known as a high-proper-motion star with $\mu_{RA} = 0.14 \pm 0.55$ mas yr^{-1}, and $\mu_{Dec} = -2.89 \pm 0.47$ mas yr^{-1} (Perryman et al. 1997). Its *Hipparcos* proper motion corresponds to a velocity of 28±8 km s^{-1} in the plane of the sky at 2000 pc. Combining this with the star's radial velocity gives a space velocity of 32±8 km s^{-1}, placing it above the nominal 30 km s^{-1} threshold for runaway status. The yellow bar in Figure 3 shows the implied sky motion (from left to right) over 10,000 years and has position angle uncertainty of about 15 degrees. The orientation of the candidate bowshock implies a velocity vector toward the lower left of Figure 3 while the proper-motion data imply a velocity that is toward the lower right.

Figure 13 shows that Bowshock 3 is detected with certainty only at [24] and longer wavelengths, with a marginal detection at [3.6] and [4.5]. The stellar SED is well fit by an early B giant (T_{eff}=25,000 K, R=10 $R_{\odot}$), consistent with its spectral type, at a distance of 1.6 kpc with an extinction $A_V = 1.0$ mag. Curiously, HD195229 has a much lower extinction than the rest of the stars in Cyg OB2 (4–6 mag), requiring either that this star is seen through a local minimum in the obscuring dust, or that HD 195229 is actually on the near side of a heavy veil of extinction that enshrouds most of Cygnus X.

The lack of similarity between the [24] appearance and the theoretical shape in Figure 14, coupled with the misalignment between the proper motion and putative bowshock morphology, casts doubt on a bowshock interpretation. We categorize the nature of this nebula as ambiguous.

3.4.4. Bowshock Candidate 4 and Star 4 (G79.4171+1.2703)

Bowshock candidate 4 resembles Bowshock 1, having no detectable emission at the IRAC bandpasses and a lima-bean morphology at [24]. Note the edge-brightened cloud to the right of the bowshock, suggesting illumination by the (presumed) early-B star powering the nebula. The central star is the faintest in our sample at optical and infrared wavelengths and Figure 12 suggests a very large extinction of $A_V > 12$. Its K-band magnitude is similar to the central star of Bowshock 2, so it is probable that this is also an early B star, if located at a similar distance. There is no literature identification for this star, so we give it a designation according to its Galactic coordinate, G79.4171+1.2703.

We note that the putative bowshock nebula points away from Cyg OB2 and in the direction of the H II region IRAS20264+4042, located toward the upper right from Star 4 in Figure 1. This star forming region is also identified as the radio source DR7 (Downes & Rinehart 1966) and the host of the ultra-compact H II region G79.320+1.313 (Kurtz et al. 1994). While it is possible that outflows from this SF region are responsible for the high relative velocities leading to the production of the putative bowshock (as shown for bowshocks in M17 and RCW 49 by Povich et al. (2008)), a careful search for other similarly oriented bowshocks around IRAS20264+4042 revealed none.

Odenwald & Schwartz (1993) report a ^{12}CO detection for IRAS20264+4042 at $V_{LSR} = -42$ km s^{-1}, corresponding to a kinematic distance of 6–7 kpc inferred from the Clemens (1985) Galactic rotation curve. However, Dutra & Bica (2001) and Le Duigou & Knödlseder

(2002) suggest distances of 1.1 and 1.6 kpc respectively, based on near infrared photometry. At such a distance, the K=11.3 magnitude of the central star, coupled with an implied extinction of A_K ~1.5 mag would correspond to an early- to mid-B star. At the the larger (but, we contend, less probable) distance of 6.5 kpc, the apparent magnitude would be consistent with an O9V or similar. Given the abundance of early-type stars at the nearer distance of Cyg OB2, we prefer the near distance and the corresponding early-to-mid B spectral type.

Figure 13 shows that Bowshock Candidate 4 is detected only at [24] and [70]. Although the stellar spectral type is not known with certainty, the stellar SED is well fit by an ~B3 dwarf (T_{eff}=20,000 K, R=4 $R_\odot$) at a distance of 1.6 kpc with a very high extinction of $A_V = 16$ mag. The stellar photometry exhibits an excess at [8.0], suggesting the presence of hot dust or possibly PAHs associated with the star. Lack of similarity to the theoretical bowshock shape leads us to classify this object as ambiguous.

3.4.5. Bowshock Candidate 5 and Star 5 (A10)

Figure 5 shows Bowshock Candidate 5 to be a stunning combination of emission at the IRAC and MIPS bandpasses. The central star is A10 in the notation of Comerón et al. (2002). Our new spectrum of A10, shown in Figure 19, is consistent with a late O star, although the uncertainty is several spectral subclasses. Its heliocentric radial velocity is 10±10 km s^{-1}, consistent with other Cyg OB2 members. Its JHK colors and magnitudes are similar to the central star of Bowshock Candidate 1, suggesting a similar reddening and late O spectral type if at the distance of Cyg OB2. The angular distance between the star and bowshock apsis is ~25″ or 0.19 pc projected separation.

Figure 13 shows that the 2MASS data are well fit by an O9V (T_{eff}=31,000 K, R=8 $R_\odot$) at a distance of 1.6 kpc with an extinction of $A_V = 7.5$ mag. The nebula dominates the SED at the IRAC and MIPS bandpasses.

Figure 14 shows that the [8.0] and [24] appearance closely resembles the theoretical bowshock shape. The orientation is consistent with either motion *toward* Cyg OB2 or interaction with a flow of material emanating from Cyg OB2. We classify this object as a probable bowshock.

3.4.6. Bowshock Candidate 6 and Star 6 (G80.7657+0.4966)

Bowshock candidate 6 exhibits strong emission at both IRAC and MIPS bandpasses in Figure 6. It lies within a complex of diffuse emission that may constitute a small H II region. The central star is extremely red, and Figure 12 suggests an extinction approaching $A_V = 18$. Accordingly, there is no literature identification or spectral type available, so we designate it by its Galactic coordinates, G80.7657+0.4963.

Though the nebular component of object 6 is strong at the IRAC and MIPS bandpasses, the central star is the faintest in the sample at IRAC bandpasses. While there is no spectral information on Star 6, if we assume it is at 1.6 kpc the 2MASS SED is well fit by a mid-B dwarf (T_{eff}=15,000 K, R=3 $R_\odot$) with a very high extinction of A_V =19 mag.

Star 6 is one of only three detected at [24], suggesting the presence of a dusty shell or disk associated with the star, since we would not expect to detect the stellar photospheres at [24] or [70]. Figure 13 shows that the flux from the star at [24] is greater than the nebular flux and continues to rise beyond 24 microns. These characteristics suggest that Star 6 is a pre-main-sequence object illuminating a rim of material that points toward Cyg OB2, the likely source of a high-velocity wind.

Figure 7 shows the [8.0] image (green), [24] image (red), and ^{12}CO (1-0) molecular line map (blue and contours) integrated between LSR velocities -7 – -3 km s^{-1} and 9 – 14 km s^{-1}(Brunt 2009). This figure shows that Bowshock 6 is located along a tendril of CO (at velocities -7 – -3 km s^{-1}) pointing toward Cyg OB2. It lies adjacent to a prominant gasseous "pillar" seen at [8.0] and in CO. The star forming region IRAS 20343+4129, which contains several pre-main-sequence B stars (Campbell et al. 2008), constitues the head of this pillar and is coincident with a concentration of CO at velocities 9 – 14 km s^{-1}. This pillar also points toward Cyg OB2, consistent with it being eroded by radiant and mechanical luminosity of the massive stars therein. The similarity between the contents (young early B stars) and morphology (pillar/CO filament) of the Star 6 region and IRAS 20343+4129 raises the intriguing possibility that these two represent different phases, and perhaps different viewing angles of the same phenomenon: massive star formation triggered in the heads of gas columns being eroded from the outside. The lack of a strong CO concentration and visible pillar of photo-dissociated material near Star 6, coupled with the presence of the bowshock pointing toward Cyg OB2 suggests that the region containing Star 6 may be at a more evolved stage compared to IRAS 20343+4129. It may also be that the stars within IRAS 20343+4129 are more massive and, thereby, generate a more luminous H II region. We classify the central star of Bowshock Candidate 6 as a probable young stellar object.

3.4.7. Bowshock Candidate 7 and Star 7 (A37)

Bowshock candidate 7 has the largest angular extent of any of our targets, covering nearly $5'$ in Figure 8. It is detected only at [24] and [70]. The central star appears to be A37 in the notation of Comerón et al. (2002). Hanson (2003) determines a spectral type of O5V((f)), making it the most energetic and massive in our sample. The presence of a bowshock associated with the this star is noted by Gvaramadze & Bomans (2008) on the basis of images from the *Midcourse Space Experiment* mission. The angular distance between the star and bowshock apsis is the largest in our sample, $\sim$70$''$, or 0.53 pc projected separation.

The SED of Star 7 in Figure 13 is consistent with an O5V star (T_{eff}=40,000 K, R=11 $R_{\odot}$) and A_V = 5 mag if placed at a distance of 2.1 kpc, slightly larger than the nominal distance to Cyg OB2, although the line-of-sight depth along the Cygnus-X complex is likely to be $\sim$few hundred pc (Odenwald & Schwartz 1993).

The excellent agreement between the [24] morphology and the theoretical shape leads us to classify this as a probable bowshock. The orientation of the bowshock indicates a motion toward the left in Figure 8, roughly tangent to the vector toward Cyg OB2. This suggests that the origin of A37 lies somewhere outside of Cyg OB2.

3.4.8. Bowshock Candidate 8 and Star 8 (G77.5168+1.9047)

Bowshock candidate 8 is visible at both IRAC and [70] bandpasses. Figure 9 shows that this object lacks the classical arc morphology and symmetry of the other bowshocks, warranting an ambiguous classification. It resembles a partial shell or bubble. The WIRO spectrum of this star obtained 2009 September 16 is consistent with a B2V – B3V having a heliocentric radial velocity of 2±4 km s^{-1}, similar to other Cyg OB2 members. The apparent central star, designated G77.5168+1.9047, is relatively bright at J=10.5, and it has 2MASS magnitudes and reddening consistent with other bowshock stars and early-type Cyg OB2 members.

Figure 13 shows that the near-IR SED of Star 8 is well fit by a B3V (T_{eff}=20,000 K, R=4 $R_{\odot}$) with A_V = 4.5 at a distance of 1.6 kpc. The IRAC and MIPS bands are dominated by extra-photospheric emission, consistent with hot dust near the star. Star 8 is one of only three stars (Star 6 and Star 9) detected at [24], suggesting the presence of dust in a circumstellar disk or envelope. The morphology of the nebula is does not bear a strong resemblance to the theoretical bowshock shape. As such, we designate Star 8 as a possible young stellar object (YSO).

3.4.9. Bowshock Candidate 9 and Star 9 (G76.8437+0.1231)

Bowshock candidate 9 is a compact nebula with detected emission only at [5.8] and longward. The central star is clearly seen as a point source in Figure 10. The stellar SED of Star 9 is difficult to ascertain, since there is no 2MASS counterpart to the point-like source detected at the mid-IR IRAC bands. The mid-IR flux rise steeply with wavelength, consistent with a heavily enshrouded source. The [4.5] flux lies below the expectations of a simple interpolation between the [3.6] and [5.8] bands. This has become a classic signature of material dominated by emission from large molecules (e.g, PAHs; Draine & Li (2007)), which are largely absent in the [4.5] band. The nebular morphology does not bear a strong resemblance to the classical bowshock shape. These characteristics are consistent with a young (class I?) protostar (Kenyon et al. 1993), and we designate this object as a probable YSO.

3.4.10. Bowshock 10 and Star 10 (GG77.0511-0.6092)

Bowshock 10, pictured in Figure 11 is a small, narrow filament with strong emission in the IRAC bands, and a low ratio of far-IR to mid-IR flux in the final panel of Figure 13. The stellar source is identified only by its Galactic coordinates, G77.0511-0.6092. Because it has similar 2MASS colors and magnitudes as many of the other bowshock stars, we consider it to be a probable late O or early B star at the distance of Cyg OB2.

The near-IR SED of Star 10 is consistent with an early B star (T_{eff}=25,000 K, R=5 $R_{\odot}$) with $A_V = 6$ at a distance of 1.6 kpc. The IRAC points lie in excess of the photosphere, consistent with hot dust and emission from PAHs. The morphology of the [8.0] nebula appears irregular, while the [24] nebula is similar to the classical bowshock morphology. We classify this object as ambigous.

3.4.11. BD+43°3654

Comerón & Pasquali (2007) present proper motions and *MSX* infrared images of the O4If star BD+43°3654, originally identified as a probable runaway by van Buren & McCray (1988) on the basis of a probable bowshock seen with IRAS.[4] They compute a distance of

---

[4]BD+43°3654 lies outside the area of the *Spitzer* Legacy Survey of the Cygnus-X Complex, so we do not discuss this object in detail or present figures.

1450 pc and propose that BD+43°3654 was ejected from Cyg OB2 1.6 Myr ago, not long after its birth. Gvaramadze & Bomans (2008) propose that BD+43°3654 is a blue straggler, formed from the merger of two stars and ejected from Cyg OB2 during a binary-binary encounter. They invoke the high proper motion pulsars B2020+28 and B2021+51 as the descendants of the other two stellar participants in this 4-body interaction.

We cross-correlated the WIYN spectrum of BD +43°3654 with an O5I model atmosphere, which yielded a heliocentric radial velocity of V_{LSR}=−66.2±9.4 km s^{-1}. This is considerably more negative than the V_{LSR}=−10 km s^{-1} mean velocity of O stars in Cyg OB2 (Kiminki et al. 2007), and therefore BD +43°3654 would qualify as a runaway on the basis of its radial velocity alone. Its motion in the plane of the sky is 39.8 ± 9.8 km s^{-1} (Comerón & Pasquali 2007) at the assumed distance. Combining this with our radial velocity measurement, we calculate the heliocentric space velocity of BD+43°3654 to be 77 ± 10 km s^{-1}.

3.5. Summary of Classifications and Statistics of Runaways in Cygnus X

The bowshock candidates presented here comprise a mixed bag of phenomena. Objects 2, 5, and 7 (and BD +43°3654) are most likely to be genuine bowshocks powered by runaway stars on the basis of having early spectral types and nebular morphologies most similar to the classical bowshock appearance. However, none of stars 2, 5 or 7 have remarkable radial velocities. Objects 1, 3 (the high proper-motion star HD195299), 4, and 10 are ambiguous, having nebular morphologies less similar to the classical bowshock shape, but, nevertheless, appear to be early-type stars. Objects 6, 8, and 9 have central stars with excess IR emission, suggesting circumstellar material. Stars 6 and 9 also have high extinction and/or SEDs that rise toward longer wavelengths, consistent their being young stellar objects hosting disks or circumstellar envelopes. The nebula associated with Star 6 shows evidence for being the head of a gaseous pillar being ablated by radiation from the direction of Cyg OB2. Hence, objects 6, 8, and 9 are the least likely to be high velocity runaway stars.

In a magnitude-selected sample of 195 bright O stars, Gies & Bolton (1986) found that 16 (8%) could be classified as runaways either on the basis of radial velocities (6; 3%), proper motions (5; 2.5%), or extreme distance from the Galactic Plane (5; 2.5%). By contrast the radial velocity survey of 146 Cyg OB2 stars by Kiminki et al. (2007) did not find any runaways. The *SST* Cygnus X Legacy Survey covers a much larger region ($\sim$ 23 square degrees) than the sample of core Cyg OB2 members studied by Kiminki et al. (2007) ($\sim$ 0.35 square degrees), which was selected from the optical imaging survey of Massey & Thompson (1991). The ratio of areas in these two surveys is roughly 65, so one might conclude that the number of early type stars in Cygnus X is as many as 146 $\times$65 = 9500. However, the earliest and most massive stars appear to be contained within the core Cyg OB2 region covered by Massey & Thompson (1991), so that this is a gross overestimate. We very conservatively adopt that the *SST* Cygnus X Legacy Survey survey includes $\sim$600 OB stars earlier than B2, or about four times the number of OB stars surveyed by Kiminki et al. (2007). In this region we find only three candidates for runaways—four if BD +43°3654 is included. At face value, this is 3/600 = 0.5%. Of course, high space velocities are a necessary but not a sufficient condition for for the formation of bowshocks. van Buren et al. (1995) found that 58 out of 188 high velocity stars evince bowshocks at IRAS sensitivity levels, and of these, 25 have well resolved structure. We expect that *SST* would detect even fainter and smaller bowshocks. If we assume that 1/4 of runaway stars produce bowshocks visible at *SST* sensitivity levels and that 8% of all OB stars are runaways, we would expect to find on the order of 12 bowshocks in the Cygnus X region. Why do we detect so few?

We identify only three probable bowshock runaways, and perhaps only one of these (Bowshock 2) has an orientation suggesting an origin near Cyg OB2. It is certainly possible that most of the runaways, like BD +43°3654, could fall outside the survey area if they have high space velocities and wereprobable ejected from the Association very early in its formation. Stars with a tangential velocity of 30 km s^{-1} would travel beyond the boundaries of the *SST* Cygnus X Legacy Survey ($\sim$26 pc diameter) in about 0.5 Myr—a small fraction of the 2–4 Myr age of Cyg OB2. Dynamical ejection scenarios wherein N-body interactions in close multiple systems expel stars would predict this—that most of the runaways are produced early in the formation of a young massive star cluster and have already traveled beyond the immediate cluster vicinity. Supernova ejection scenarios, on the other hand, predict that the start of the ejection process is delayed several Myr (until the explosion of the most massive stars), and then it continues at a constant or increasing rate as stars from lower-mass OB binaries complete their evolution. Although the arguments are mostly qualitative, our findings would seem to be more consistent with the dynamical ejection scenario.

4. Bowshocks and Laboratories

Baranov et al. (1971) first articulated the theoretical basis for momentum-driven bowshocks in the context of the solar wind termination shock. The theory of stellar wind bowshocks has since been further refined in papers by van Buren & McCray (1988), van Buren et al. (1990), Wilkin (1996), Wilkin (2000) and simulated numerically by Comerón & Kaper (1998). A bowshock forms at a radial distance R_0 where the momentum flux from the stellar wind material of density ρ_w and velocity V_w is equal to the momentum flux from the ambient medium of density ρ_a moving at V_a relative to the star. The relative velocity may be the result either of a "runaway" star moving at high speed or a bulk flow of the ISM, such as an outflow from a young star-forming region. Hence,

$$\frac{1}{2}\rho_w V_w^2 = \frac{1}{2}\rho_a V_a^2. \tag{1}$$

The density of the stellar wind can be expressed as

$$\rho_w = \frac{\dot{M}_w}{4\pi R_0^2 V_w} \quad , \tag{2}$$

where $\dot{M}_w$ is the stellar mass loss rate. It follows that the standoff distance of the bowshock is

$$R_0 = \sqrt{\frac{V_w \dot{M}_w}{4\pi \rho_a V_a^2}} \quad . \tag{3}$$

R_0 can be measured directly from the bowshock images, assuming that all of the stars are located at the adopted distance of Cyg OB2. Technically, only the projected separation, R_0 *cos* i, can be measured, but in order to observe a bowshock morphology, the viewing angle cannot be far from $i = 0°$ so that *cos* i is not far from unity. Adopting a mean ISM gas mass per H atom of $\mu = 2.3 \times 10^{-24}$ g means that ρ_a can be expressed in terms of the ambient number density: $\rho_a = \mu n_a$. Stellar wind speeds and mass loss rates have proved difficult to measure and may be even more uncertain than previously believed (Puls et al. 2008; Fullerton et al. 2006). As an estimate of the mass loss rates and wind velocities for stars in our sample, we adopt the values tabulated by Mokiem et al. (2007) for early type stars. Equation 3 can then be rearranged to yield the relative motion btween the star and ambient medium,

$$V_a = \sqrt{\frac{V_w \dot{M}_w}{4\pi R_0^2 \mu}} n_a^{-1/2} \quad . \tag{4}$$

In practice, it is difficult to calculate the star's velocity, V_a, relative to the surrounding medium because the quantities on the right hand side are poorly known, especially the density of the ambient medium, n_a. By adopting published estimates for the stellar mass loss rates and wind velocities, we can at least make an estimate of the product V_a $n_a^{1/2}$, similar to the approach of Povich et al. (2008). In keeping with the precedent established in van Buren & McCray (1988) and Povich et al. (2008), we write the mass loss rate in units of 10^{-6} $M_{\odot}$ yr^{-1} as $\dot{M}_{w,-6}$, the stellar wind velocity in units of 10^8 cm s^{-1} as $V_{a,8}$ and the ambient medium density in units of 10^3 cm^{-3} as $n_{a,3}$. The relative star-ISM velocity is then,

$$V_a = 1.5(\frac{R_0}{pc})^{-1}(V_{w,8}\ \dot{M}_{w,-6})^{1/2} n_{a,3}^{-1/2} \quad [km\ s^{-1}]. \tag{5}$$

Given the uncertainties in stellar mass loss rates and wind velocities for stars later than about B0, we compute and tabulate derived parameters only for the five objects in our sample with the most reliable spectroscopic types, objects 1, 3, 5, 7, and 11 (BD+43°3654). Table 3 tabulates the adopted stellar wind velocities, mass loss rates (from the works of Repolust et al. (2004); Mokiem et al. (2005); Martins et al. (2005); Crowther et al. (2006), as summarized in Mokiem et al. (2007)), standoff distances, R_0 *cos i*, along with the product $V_a\ n_{a,3}^{1/2}$. The standoff distances of 0.11 – 1.8 *cos i* pc are consistent with those found for the bowshocks in Povich et al. (2008). The derived values for $V_a\ n_{a,3}^{1/2}$ lie in the range 0.2 to as much as 30 — broadly consistent with the values from the (Povich et al. 2008) stars. For typical ISM densities of $n_{a,3}$=0.1 – 1.0, the implied stellar speeds are few×10 km s^{-1}, consistent with the expected speeds of runaway stars.

4.1. A Novel Measure of Stellar Mass Loss Rates

Because stellar mass loss rates are probably the most uncertain parameter in Equation 5 above, we invert the approach taken by Povich et al. (2008) and exploit the phenomenon to yield an estimate of the mass loss rates for the central stars. Inverting Equation 5 yields the mass loss rate of the star as a function of the relative motion between the str and ISM, the ambient density, the stellar wind speed, and the standoff distance,

$$\dot{M}_{w,-6} = \frac{0.67[R_0(pc)]^2[V_a(km/s)]^2 n_{a,3}}{V_{w,8}}\ . \tag{6}$$

R_0 is readily observed from the bowshock images, assuming a 1.6 kpc distance to Cygnus X and assuming *cosi* $\simeq 1$. We assume a minumum star–ISM speed of V_a=30 km s^{-1} for runaway stars (Gies & Bolton 1986), and we adopt the stellar wind speeds of Mokiem et al. (2007) which, for our sample of O5 – B0 stars, range from 3000 km s^{-1} to ∼800 km s^{-1} ($V_{w,8}$=3 to <0.8). The ambient number density, $n_{a,3}$, is difficult to measure directly, but may be estimated from $n_{s,3}$, the post-shock density within the luminous bowshock nebulae. For strong, highly supersonic shocks, $n_{s,3} \simeq 4n_{a,3}$ (Landau & Lifshitz 1987). Without knowing the Mach number of each individual case, we adopt $n_{s,3} = 2n_{a,3}$, and consider the uncertainties to be factors of 2–4. We estimate $n_{s,3}$ by fitting the bowshock spectral energy distributions in Figure 13 with the dust/PAH models of Draine & Li (2007) which give the dust emissivity per H nucleon as a function of the radiation field intensity, parameterized as a multiple, U, times the mean interstellar radiation field of U_{ISRF}=2.3×10^{-2} erg s^{-1} cm^{-2} (Mathis et al. 1983). We make the motivated assumption that the bowshock luminosity stems from reprocessed photons from the central star rather than thermalized mechanical energy from the stellar wind (Benjamin 2009). The appropriate choice of model radiation field intensity, U, is then the ratio of the flux from the central star at the standoff distance over the mean interstellar field, estimated as,

$$U = \frac{R_*^2 \sigma T_*^4}{R_0^2} \, U_{ISRF}^{-1} \ , \tag{7}$$

where R_* is the stellar radius, T_* the effective stellar temperature, and σ the usual Stefan-Botlzmann constant. The postshock number density can then be estimated as

$$n_{s,3} = 10^{-3} \frac{N}{V} \ , \tag{8}$$

where V is the bowshock volume which we estimate by approximating the bowshocks as hollow cones at a known distance, D, and $N = L_{obs}/L_0$, the ratio of the observed luminosity at a given bandpass to the theoretical luminosity per nucleon in the Draine & Li (2007) models. Effectively, $n_{s,3}$ is found empirically because it is the scale factor by which we multiply the Draine & Li (2007) models to match the observed SED. Because $V \propto D^3$ and the inferred luminosity $L_{obs} \propto D^2$, our estimate for $n_{s,3}$ varies as D^{-1}, inversely with the adopted distance.

Draine & Li (2007) parameterize the model spectral energy distributions in terms of a maximum and minimum radiation field indicent on the dust, U_{max} and U_{min}. While dust in the typical ISM is exposed to a range of intensities, we expect that material in the bowshocks is irradiated by a single intensity dictated by the stellar luminosity and standoff distance. Therefore, we adopt the models with $U_{max} = U_{min} \equiv U$, where U is chosen according to Equation 7. Figure 13 of Draine & Li (2007) shows that the flux ratio [24]/[70] is sensitive to U over the range $1 < U < 10^7$, and we make use of this sensitivity in fitting the bowshock SEDs below. We adopt the models appropriate to Milky Way dust and leave the PAH fraction, q_{PAH}, as a free parameter. Larger values of q_{PAH} raise the flux in the IRAC bandpasses where PAH emission is strong, but have no effect on the SED at [24] and [70].

Dotted lines in Figure 13 show illustrative dust models that provide reasonable fits to the mid- and far-IR data. The slope of the SED between [24] and [70] allows us to guess the appropriate value for U *without* any prior knoweldge of the the stellar luminosity or R_0. Interestingly, the values for U in each case calculated from Equation 7 are generally within factors of 2–3 of the initial guess. This correspondance serves as a kind of corroborating evidence that the bowshocks are, in fact, powered by the radiant energy from their central stars. The fits of the models to the data in Figure 13 are done by eye to maximize the agreement at [24] and [70] by adjusting $n_{s,3}$, and then the parameter q_{PAH} is varied to achieve a best fit at the IRAC bands. The models provide reasonably good fits to the data for objects 3, 5, & 8. In other cases, the overall fit is poor at the IRAC bandpasses because the model PAH features are too weak, even for the maximum model q_{PAH}, or too weak, even for the minimum model q_{PAH}. We take these discrepancies as indications that PAHs may be destroyed in the bowshocks (former case; objects 1, 4, & 7), and that PAH excitation may be elevated and dominate the SED in some objects (latter case; objects 2 & 6). The adopted values for U and $n_{s,3}$ appear in each panel.

Armed with estimates of the ambient number densities, $n_{a,3} = 1/2n_{s,3}$, we proceed to calculate mass loss rates, $\dot{M}_{w,-6}$, using the method outlined above. Again, we consider only the four objects with the most reliable spectroscopic types where the bowshock nature is more likely to be correct. Table 4 summarizes the relevant parameters adopted for each of objects (2, 5, 7, 11). Derived mass loss rates vary from $< 0.18 \times 10^{-6}$ $M_\odot$ yr^{-1} for the early B star (Star 2) to $\sim 1 \times 10^{-6}$ $M_\odot$ yr^{-1} for the O9V star (Star 5), to $\sim 3 \times 10^{-6}$ $M_\odot$ yr^{-1} for the O5V star (A37). The O4If star BD+43°3654 stands out, having an implied mass loss rate of 160×10^{-6} $M_\odot$ yr^{-1}. This large value results from the rather large standoff distance, $R_0 = 1.4$ pc, implied by the *MSX* infrared image from Comerón & Pasquali (2007). We note that we have no direct measure of the ambient ISM density for this object, so we have assumed the average value from the other four early type bowshock stars. Results for BD+43°3654 should be regarded as particularly uncertain. These results are broadly consistent with the mean $\dot{M}$ values for mid- to late-O stars estimated by Lamer & Leitherer (1993); Fullerton et al. (2006) but a factor of several or more larger than the more recent compilation of Mokiem et al. (2007).

We consider the uncertainties on mass loss rates to be factors of 2–4, dominated by the uncertainties on $n_{a,3}$, which are of the same magnitude. The other parameters that appear in Equation 6 are likely known to $\sim$30%, so that uncertainties in the standoff distance, which enter as R_0^2 and V_a^2, do not have a major impact on the result. We present the calculation of mass loss rates in this section as an outline of a novel method without claiming that this approach is in any sense superior to other well-established techniques.

5. Conclusion

We have identified ten candidate bowshock nebulae and their central stars in the region surrounding Cyg OB2 on the basis of mid-IR morphologies. We provide the first spectral types and radial velocities for several stars (objects 1, 2, 5, & 8) from this survey, showing that they are late-O or early B dwarfs. We find HD195229 to be a likely runaway on the basis of its space velocity calculated from both radial velocity measurements and Hipparcos proper motions, but the velocity vectors implied by the proper motion data and bowshock orientation are nearly orthogonal. We measure the radial velocity of the suspected runaway O4If star BD+43°3654 to be $V_{helio} = -66 \pm 4$ km s^{-1}, supporting its runaway status. Based on the morphologies, spectral types, and spectral energy distributions, we identify three objects (6, 8, 9) as probable B-star young stellar objects with circumstellar material. Objects 2, 5, and 7 are probable bowshocks based on similarity to the theoretical shape. These stars, however, have modest radial velocities, consistent with those of other Cyg OB2 members, indicating that their motions must be predominantly tangential to the line of sight. Without proper motion data, we are not able to confirm a runaway status or suggest an origin for these stars. The physical nature of the nebulae around stars 1, 3, 4, and 10 remains ambiguous with the current data. These nebulae may be partial shells, partial bubbles, or rims of nearby clouds illuminated by the early-type stars. As part of our analysis, we have also proposed a novel method for determining the mass loss rates for runaway OB stars using bowshock physics that yield reasonable, if slightly larger values for $\dot{M}$ compared to more traditional methods.

We would like to thank the time allocation committees for the WIYN and WIRO observatories for graciously allowing us the observing time that made this project possible. We also thank the National Science Foundation for support provided through the Research Experience for Undergraduates (REU) grant AST 03-53760. We also thank Heather Choi for assisting with the observing run at WIRO. Bob Benjamin and Matt Povich provided helpful feedback on early drafts of this manuscript. Chris Brunt graciously allowed us early access to the CO survey of Cygnus X. Advice from an astute referee strengthened the analysis herein.

This publication makes use of data products from the Two Micron All Sky Survey, which is a joint project of the University of Massachusetts and the Infrared Processing and Analysis Center/California Institute of Technology, funded by the National Aeronautics and Space Administration and the National Science Foundation.

Facilities: WIRO (), Spitzer () , WIYN ()

REFERENCES

Bally, J., O'Dell, C. R., & McCraughrean, M. J. 2000, AJ, 119, 2919

Baranov, V. B., Krasnobaev, K. V., & Kulikovskii, A. G. 1971, Soviet Physics Doklady, 15, 791

Benjamin, R. 2009, private communication

Blaauw, A. 1961, Bull. Astron. Inst. Netherlands 15, 265

Brown, D., & Bomans, D. J. 2005, A&A, 439, 183

Brunt, C. 2009, private communication

Campbell, M. F., et al. 2008, ApJ, 673, 954

Cardelli, J. A., Clayton, G. C., & Mathis, J. S. 1989, ApJ, 345, 245

Clemens, D. P. 1985, ApJ, 295, 422

Comeron, F., & Kaper, L. 1998, A&A, 338, 273

Comerón, F. & Pasquali, A. 2007, A&A, 467, L23

Comerón, F., et al. 2002, A&A, 389, 874

Conti, P. S., Leep, E. M., & Lorre, J. J. 1977, ApJ, 214, 759

Crowther, P. A., Lennon, D. J., & Walborn, N .R. 2006, A&A, 446, 279

Downes, D., & Rinehart, R. 1966, ApJ, 144, 937

Draine, B. T., & Li, A. 2007, ApJ, 657, 810

Dutra, C. M., & Bica, E. 2001, A&A, 376, 434

Dyson, J. 1975, Ap&SS, 35, 299

Gies, D. R. 1987, ApJS, 64, 545

Gies, D. R., & Bolton, C. T. 1986, ApJS, 61, 419

Gvaramadze, V. V. & Bomans, D. J. 2008, A&A, 485, L29

Fazio, G. G., et al. 2004, ApJS, 154, 10

Fullerton, A. W., Massa, D. L., & Prinja, R. K. 2006, ApJ, 637, 1025

Hanson, M. M. 2003, ApJ, 597, 957

Hester, J. J., et al. 1996, AJ, 111, 2349

Hoogerwerf, R., de Bruijne, J. H. J., & de Zeeuw, P. T. 2000, ApJ, 544, L133

Hora, J. L., et al. 2007, Massive Star Formation: Observations Confront Theory

Huthoff, F., & Kaper, L. 2002, A&A, 383, 999

Indebetouw, R., Robitaille, T. P., Whitney, B. A., Churchwell, E., Babler, B., Meade, M., Watson, C., & Wolfire, M. 2007, ApJ, 666, 321

Jacoby, G. H. & Hunter, D. A. 1984, ApJS, 56, 257

Jenniskens, P., & Désert, F. X. 1994, Astronomy & Astrophysics Suppliment Series, 106, 39

Kenyon, S. J., Calvet, N., & Hartmann, L. 1993, ApJ, 414, 676

Kiminki, D. C., et al. 2007, ApJ, 664, 1120

Knödlseder, J. 2000, A&A, 360, 539

Kurtz, S., Churchwell, E., & Wood, D. O. S. 1994, ApJS, 91, 659

Lamers, H. G. J. L. M., & Leitherer, C. 1993, ApJ, 412, 771

Landau, L. D., & Lifshitz, E. M. 1987, *Fluid Mechanics*, Pergamon Press, New York

Lanz, T., & Hubeny, I. 2003, ApJS, 146, 417

Le Duigou, J.-M., & Knödlseder, J. 2002, A&A, 392, 869

Leonard, P. J. T., & Duncan, M. J. 1988, AJ, 96, 222

Leonard, P. J. T., & Duncan, M. J. 1990, AJ, 99, 608

Marigo, P., Girardi, L., Bressan, A., Groenewegen, M. A. T., Silva, L., & Granato, G. L. 2008, A&A, 482, 883

Martins, F., Schaerer, D., & Hillier, D. J. 2005, A&A, 436, 1049

Markova, N., & Puls, J. 2008, A&A, 478, 823

Massey, P., & Thompson, A. B. 1991, AJ, 101, 1408

Mathis, J. S., Mezger, P. G., & Panagia, N. 1983, A&A, 128, 212

Mdzinarishvili, T. G., & Chargeishvili, K. B. 2005, A&A, 431, L1

Mokiem, M. R., de Koter, A., Puls, J., et al. 2005, A&A, 441, 711

Mokiem, M. R., et al. 2007, A&A, 473, 603

Noriega-Crespo, A., van Buren, D., & Dgani, R. 1997, AJ, 113, 780

Odenwald, S. F., & Schwartz, P. R. 1993, ApJ, 405, 706

Perryman, M. A. C., et al. 1997, A&A, 323, L49

Povich, M. S., Benjamin, R. A., Whitney, B. A., Babler, B. L., Indebetouw, R., Meade, M. R., & Churchwell, E. 2008, ApJ, 689, 242

Puls, J., Vink, J. S., & Najarro, F. 2008, A&A Rev., 16, 209

Reddish, V. C., Lawrence, L. C., & Pratt, N. M. 1966, Publications of the Royal Observatory of Edinburgh, 5, 111

Repolust, T., Puls, J., Herrero, A. 2005, A&A, 415, 349

Rieke, G. H., et al. 2004, ApJS, 154, 25

Schneider, N., Bontemps, S., Simon, R., Jakob, H., Motte, F., Miller, M., Kramer, C., & Stutzki, J. 2006, A&A, 458, 855

Schulte, D. H. 1958, AJ, 128, 41

Stone, R. C. 1982, ApJ, 261, 208

Strutskie, R. M. et al. 2006, ApJ, 131, 1163

Torres-Dodgen, A. V., Carroll, M., & Tapia, M. 1991, MNRAS, 249, 1

van Buren, D., Mac Low, M.-M., Wood, D. O. S., & Churchwell, E. 1990, ApJ, 353, 570

van Buren, D., & McCray, R. 1988, ApJ, 329, L93

van Buren, D., Noriega-Crespo, A., & Dgani, R. 1995, AJ, 110, 2914

Vink, J. S., de Koter, A., & Lamers, H. J. G. L. M. 2001, A&A, 369, 574

Walborn, N. R., & Fitzpatrick, E. L. 1990, PASP, 102, 379

Whitney, B. A., et al. 2004, ApJS, 154, 315

Wilkin, F. P. 1996, ApJ, 459, L31

Wilkin, F. P. 2000, ApJ, 532, 400

Table 1. Stellar Sources Associated with Bowshock Candidates

#	R.A. (J2000)	Dec (J2000)	ℓ	b	J (mag)	H (mag)	K (mag)	[3.6] (mJy)	[4.5] (mJy)	[5.8] (mJy)	[8.0] (mJy)	[24] (mJy)	S.T.	V_{helio} (km s^{-1})	Name
1	20:34:28.9	+41:56:17.0	80.8621	0.9749	9.02(0.02)	8.45(0.01)	8.21(0.01)	138(2)	91(2)	79(4)	47(4)	···	O9V[a]	-17±6	GSC03161-01188
2	20:34:34.5	+41:58:29.3	80.9020	0.9828	11.35(0.02)	10.78(0.02)	10.51(0.02)	32(2)	35(3)	74(6)	161(8)	···	B1V–B3V[a]	-12±15	G80.9020+0.9828
3	20:28:30.2	+42:00:35.2	80.2632	1.9137	7.34(0.02)	7.36(0.01)	7.32(0.02)	287(8)	204(7)	126(6)	64(4)	···	B0.2III[a]	-3±2	HD195299
4	20:28:39.4	+40:56:51.0	79.4172	1.2703	14.25(0.03)	12.31(0.02)	11.32(0.01)	19(2)	14(2)	10(3)	17(2)	···	B2V–B3V[b]	···	G79.4172+1.2703
5	20:34:55.1	+40:34:44.0	79.8224	0.0959	9.54(0.02)	8.70(0.02)	8.25(0.02)	185(2)	127(3)	96(4)	131(6)	···	O9V[a] ···	-10±10	A10[c]
6	20:36:13.3	+41:34:26.1	80.7657	0.4966	16.04(0.08)	13.90(0.06)	12.76(0.03)	23(2)	35(4)	68(4)	133(6)	1245(24)	B4V–B6V[b] ···	···	G80.7657+0.4966 (YSO?)
7	20:36:04.4	+40:56:13.0	80.2400	0.1354	8.56(0.03)	7.97(0.01)	7.68(0.02)	376(3)	141(2)	135(7)	54(3)	···	O5V[a]	···	A37[c]
8	20:20:11.6	+39:45:30.1	77.5168	1.9047	10.5 (0.02)	10.00(0.02)	9.71(0.01)	34(2)	26(2)	59(4)	157(8)	4600(80)	B1V–B3V[a]	2±4	G77.5168+1.9047 (YSO?)
9	20:25:43.9	+38:11:13.2	76.8437	0.1231	···	···	···	8(2)	20(3)	41(2)	63(3)	677(12)	B??[b]	···	G76.8437-0.1231 (YSO?)
10	20:29:22.1	+37:55:44.3	77.0511	-0.6092	10.33(0.02)	9.63(0.02)	9.27(0.01)	74(7)	49(9)	50(3)	81(5)	···	B1V–B2V[b]	···	G77.0511-0.6092
11	20:33:36.1	+43:59:07.4	82.4100	2.3254	6.64(0.02)	6.19(0.02)	5.97(0.02)	···	···	···	···	···	O4If[a]	-66±4	BD+43°3654

[a]Spectral type based on spectroscopic identification.

[b]Spectral type adopted by assuming a main-sequence star consistent with the near-IR SED if at the nominal 1.6 kpc distance of Cygnus X.

[c]Comerón et al. (2002)

Table 2. Photometry of Bowshock Candidates

#	[3.6] (mJy)	$\sigma_{[3.6]}$ (mJy)	[4.5] (mJy)	$\sigma_{[4.5]}$ (mJy)	[5.8] (mJy)	$\sigma_{[5.8]}$ (mJy)	[8.0] (mJy)	$\sigma_{[8.0]}$ (mJy)	[24] (mJy)	$\sigma_{[24]}$ (mJy)	[70] (mJy)	$\sigma_{[70]}$ (mJy)
1	<36	···	< 35	···	< 73	···	< 122	···	5100	1020	1220	250
2	78	16	88	18	328	65	795	159	539	108	10300	2060
3	20	10	19	10	<14	···	< 20	···	1370	274	659	132
4	< 5	···	< 6	···	< 5	···	< 12	···	1900	380	2900	580
5	78	16	92	18	158	32	1288	257	65300	13000	73000	14600
6	160	32	100	20	1480	296	3900	780	··· [a]	···	10970	2190
7	<26	···	< 21	···	< 23	···	< 67	···	47220	9440	35300	7060
8	71	14	88	18	214	43	570	114	2394	478	15400	3080
9	< 4	···	< 4	···	46	10	118	24	276	57	3800	760
10	21	4	24	5	32	7	100	20	1878	360	182	36

Note. — Uncertainties are estimated at 20% in all cases except nondetections where 1σ upper limits are given.

[a]High and variable background precludes a reliable measurement at [24] for this source.

Table 3. Calculated Bowshock Parameters for Most Reliable Objects

#	S.T.	R_0 *cos i* (pc)	$\dot{M}_{w,-6}$ (10^{-6} $M_\odot$ yr^{-1})	$V_{w,8}$ (10^8 cm s^{-1})	$V_a n_a^{1/2}$ (km s^{-1} (10^3 cm^{-3})$^{\frac{1}{2}}$)
2	B1V–B3V[c]	0.07	0.0003 - 0.001	<0.8	<0.68
5	O9V[a]	0.19	0.0003 - 0.1	0.8 – 1.5	0.12 – 3
7	O5V[a]	0.53	0.2 – 0.9	2.8 – 3.2	2 – 5
11	O4If[a]	1.4[b]	8	2.2	11

[a]Based on spectroscopic identification.

[b]Based on the images of Comerón & Pasquali (2007) and adopted 1.6 kpc distance.

Table 4. Derived Mass Loss Rates for Most Reliable Objects

#	S.T.	$n_{s,3}$ (10^3 cm^{-3})	$\dot{M}_{w,-6}$ (10^{-6} $M_\odot$ yr^{-1})
2	B1V–B3V	0.10	<0.18
5	O9V	0.1	0.75 - 1.3
7	O5V	0.10	2.5 – 3
11	O4If	0.10[a]	160

[a]Not measured; value adopted from the average of othe ther stars.

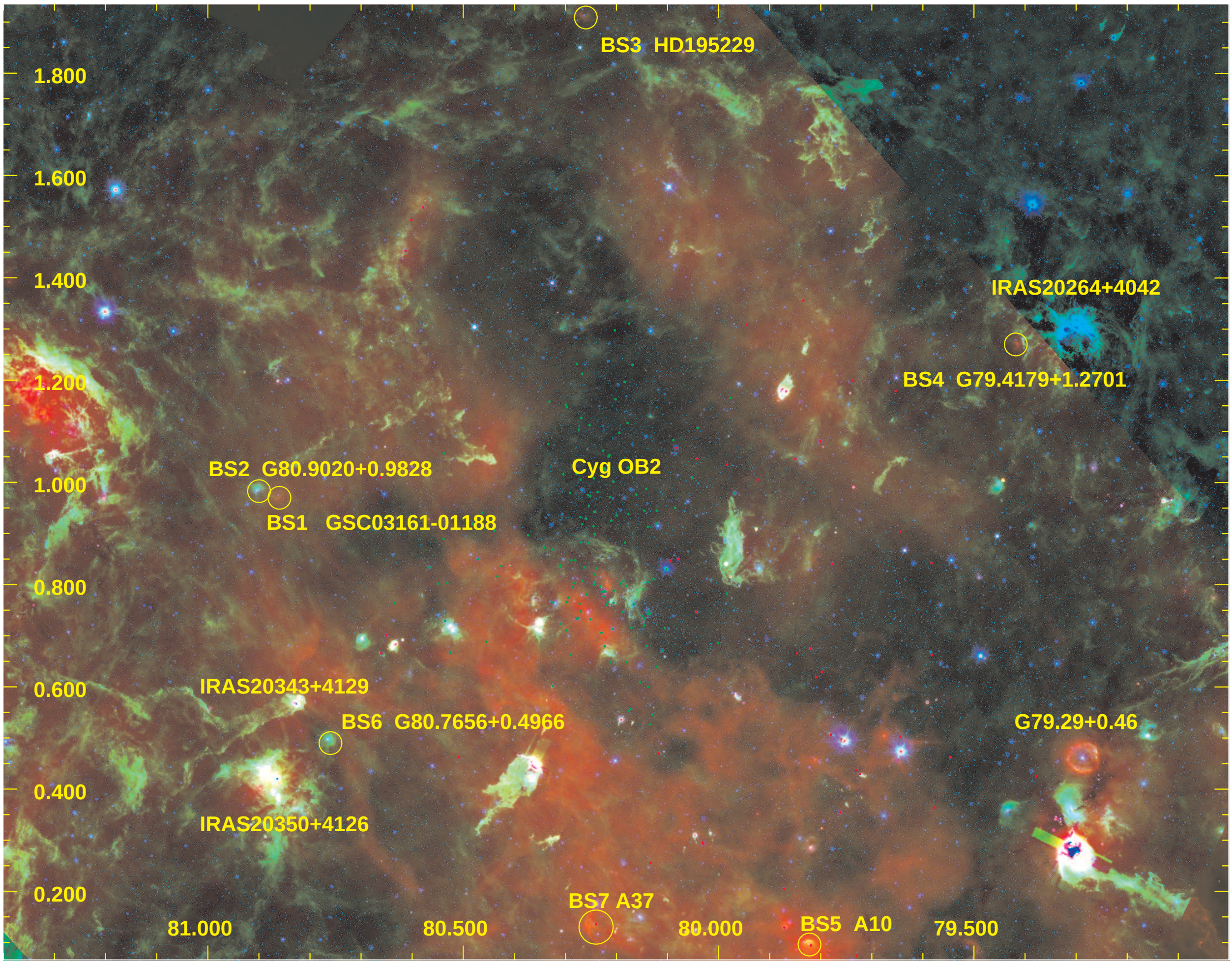

Fig. 1.— *Spitzer* three-color image in Galactic coordinates of the Cygnus-X region centered on Cygnus OB2 with [4.5] in blue, [8.0] in green, and [24] in red. Seven of the ten bowshock candidates are labeled with their bowshock number and identifications for the central stars from Table 1. Several other prominent IRAS infrared sources are labeled, some of which are the heads of gaseous pillars pointing toward Cyg OB2, such as IRAS20343+4129.

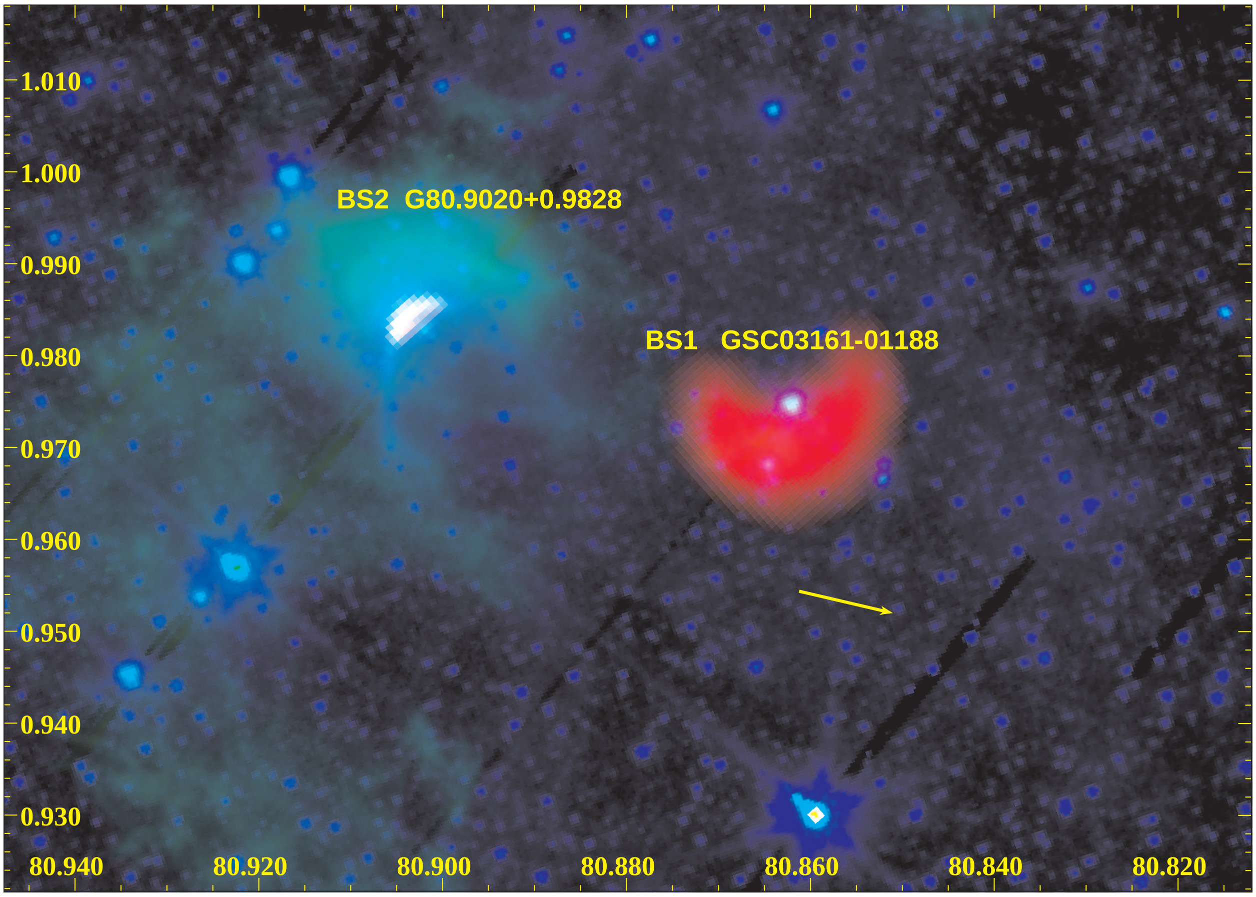

Fig. 2.— *Spitzer* three-color image of Bowshock Candidates 1 (GSC03161-01188) and 2 (G80.9020+0.9828) with the same color scheme as Figure 1. These two objects present a striking contrast as Bowshock 1 is seen only at 24 microns and longer wavelengths while Bowshock 2 has strong PAH emission in the IRAC bands and is weaker at longer wavelengths. The arrow shows the direction toward the core of Cyg OB2.

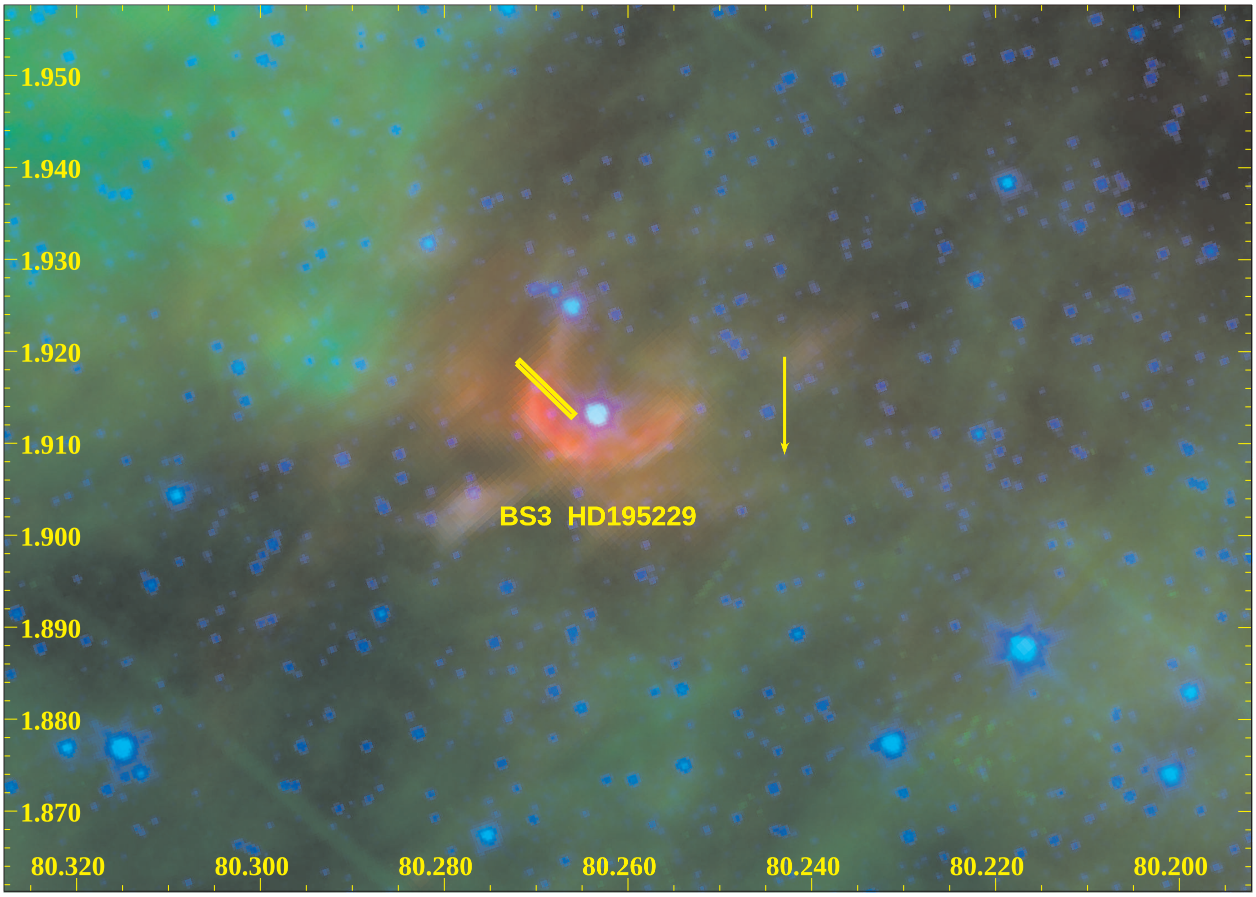

Fig. 3.— Three-color image as in Figure 1 showing the bowshock candidate around Star 3 (HD195229). The yellow line indicates HD195229's proper *Hipparcos* motion, indicating that there is a misalignment between the velocity vector inferred from proper motion data and the vector inferred from the putative bowshock morphology. The uncertainty on the position angle of the proper motion is ∼15°.

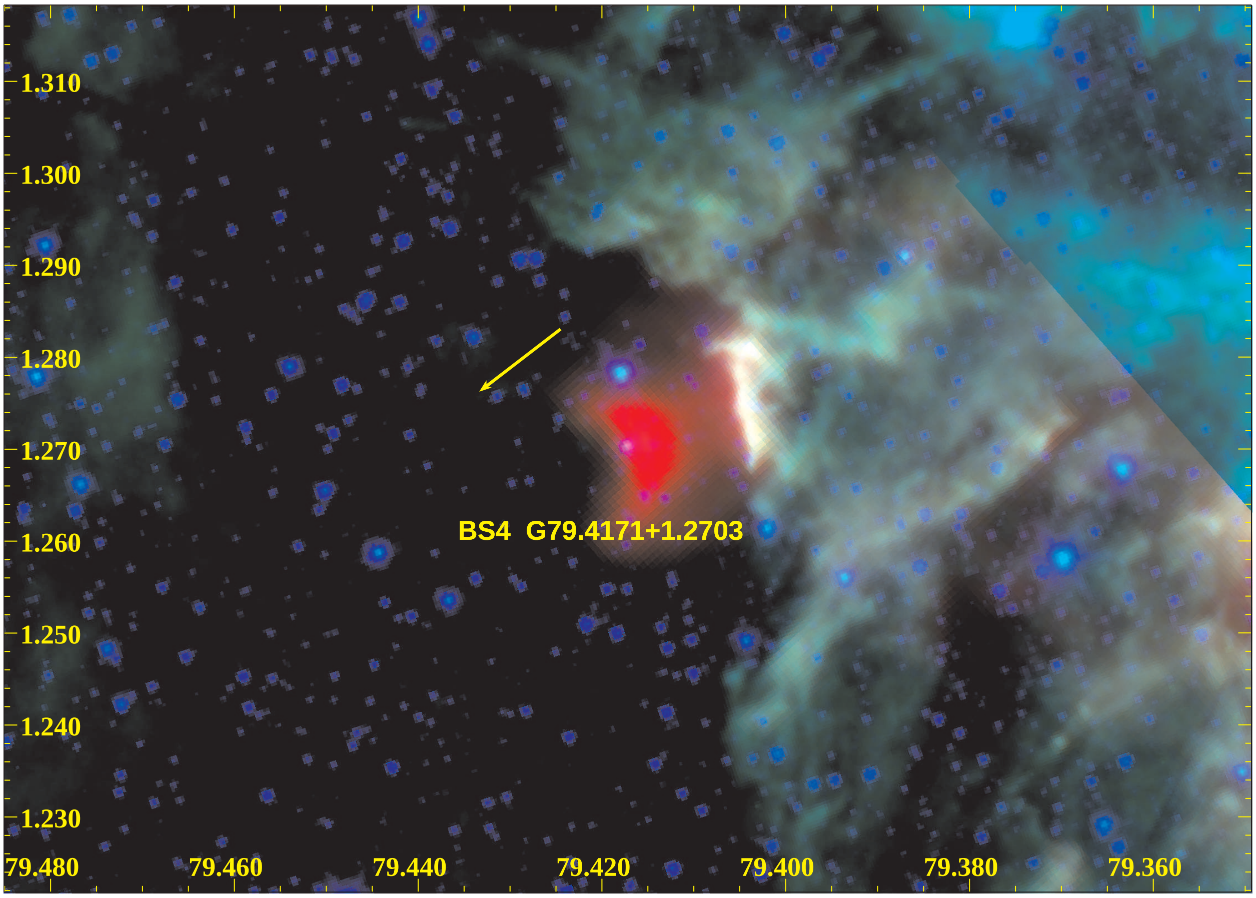

Fig. 4.— Three-color image of Bowshock Candidate 4, as in Figure 1.

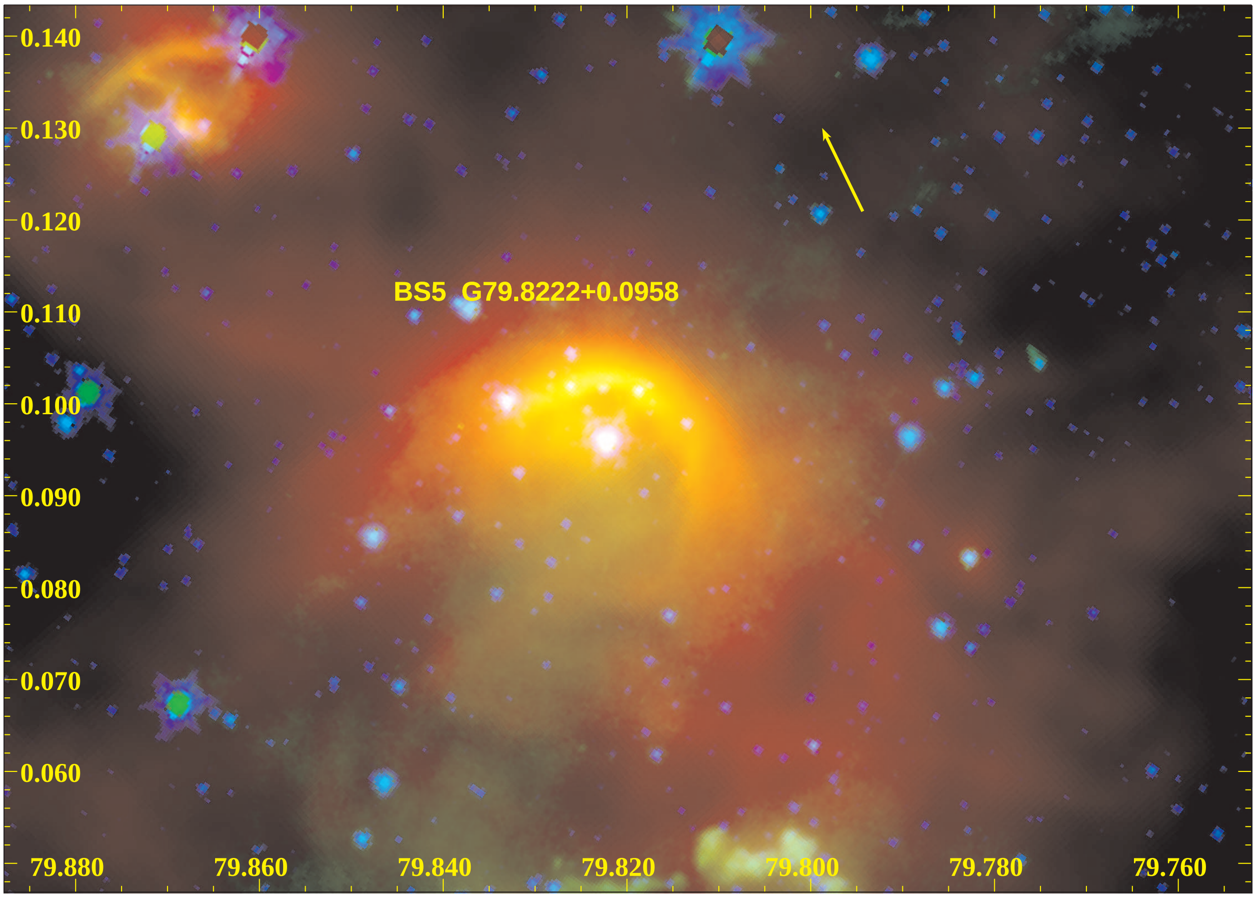

Fig. 5.— Three-color image of Bowshock Candidate 5, as in Figure 1.

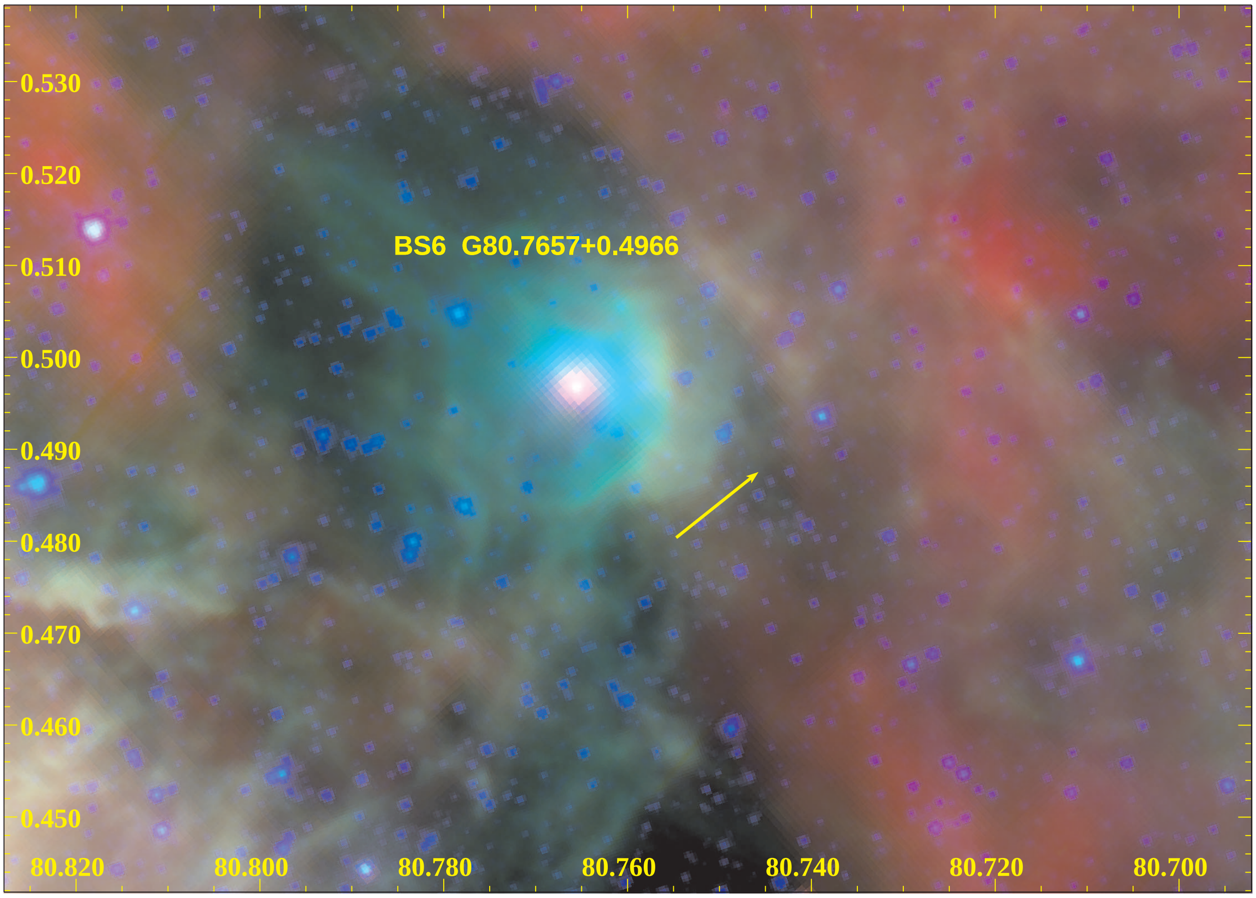

Fig. 6.— Three-color image of Bowshock Candidate 6, as in Figure 1.

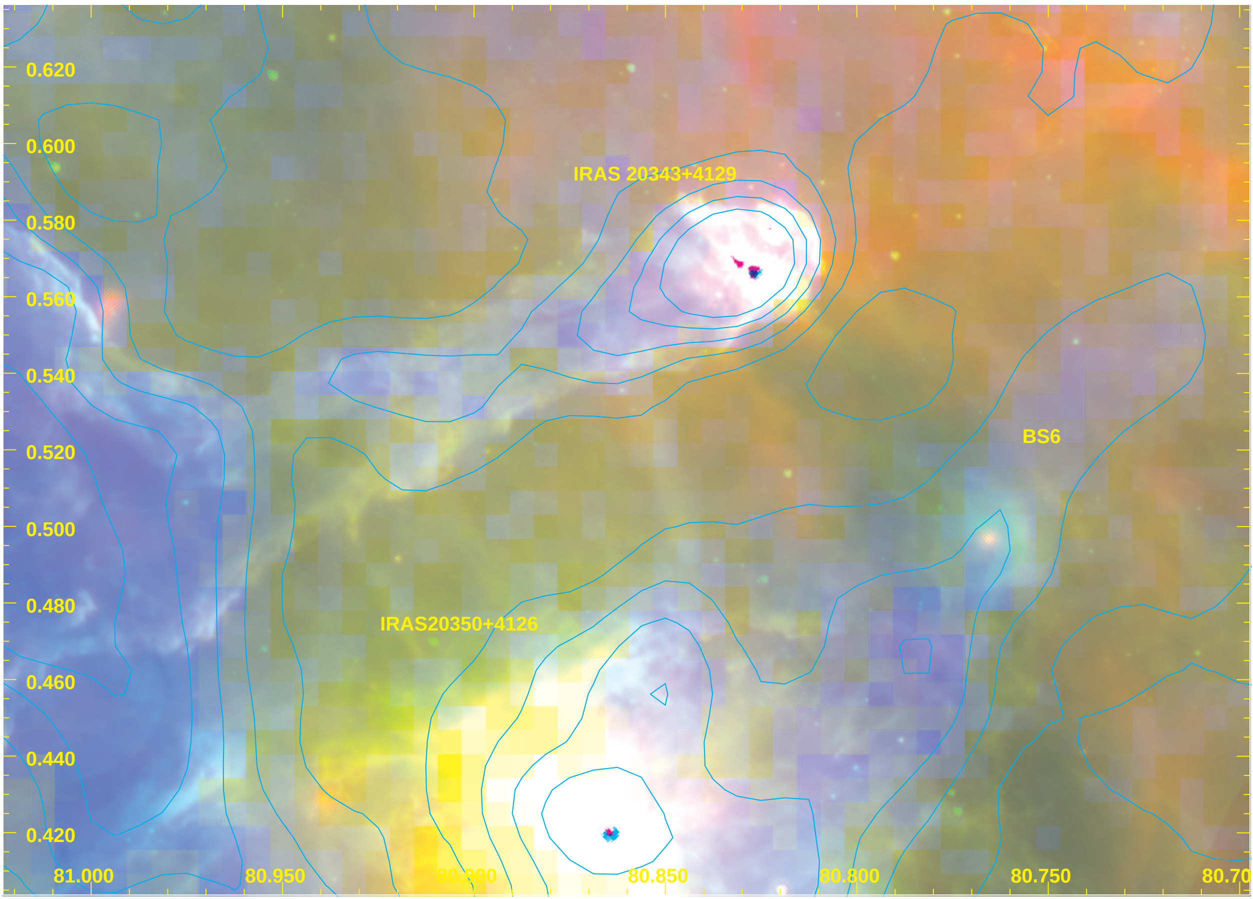

Fig. 7.— Three-color image of Bowshock Candidate 6, with [8.0] in green, [24] in red, and the ^{12}CO (1-0) map between LSR velocities -7 – -4 and 9 – 14 km s^{-1} in blue and contours. Star 6 and Bowshock Candidate 6 lie adjacent to a gasseous pillar containing several massive young protostellar objects at its head (IRAS 20343+4129).

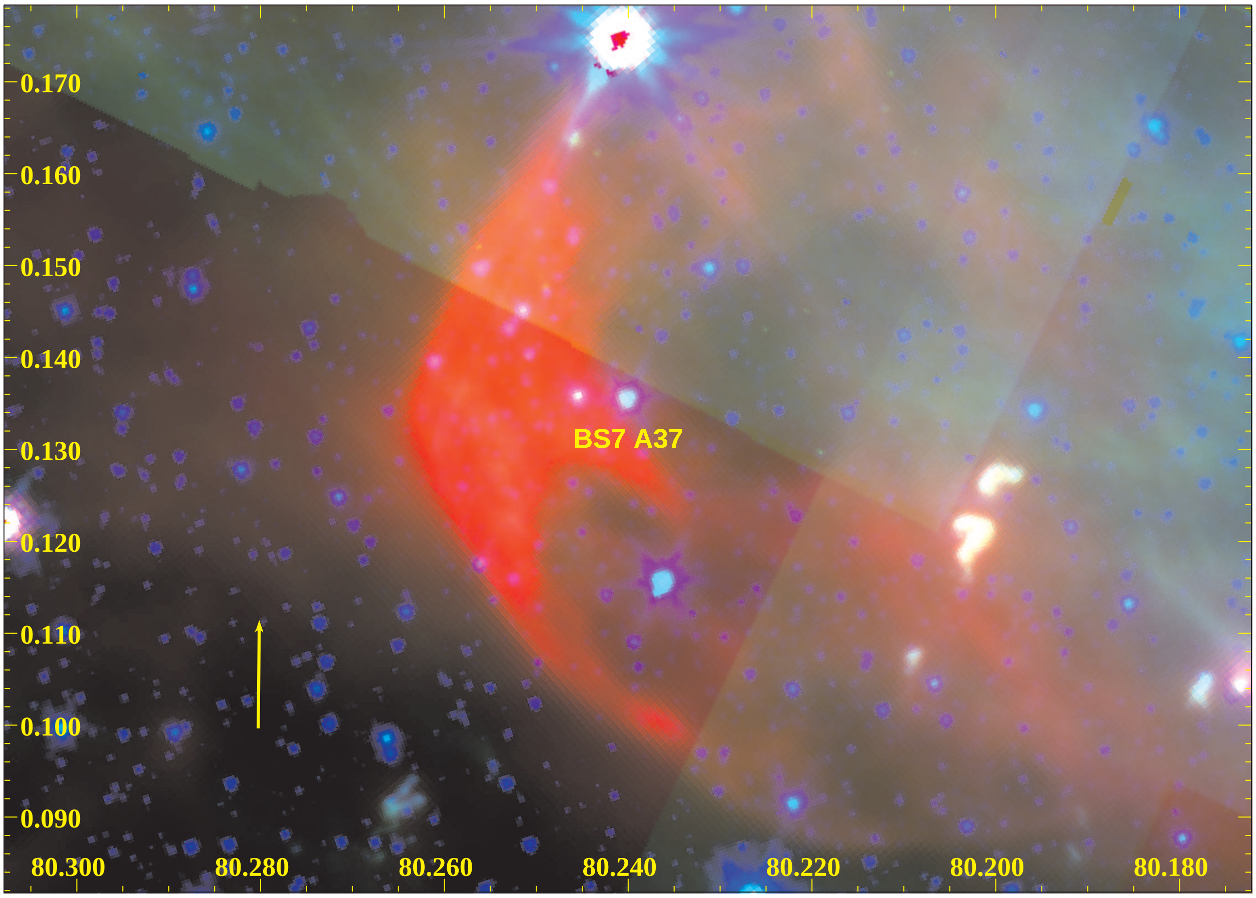

Fig. 8.— Three-color image of Bowshock Candidate 7, as in Figure 1.

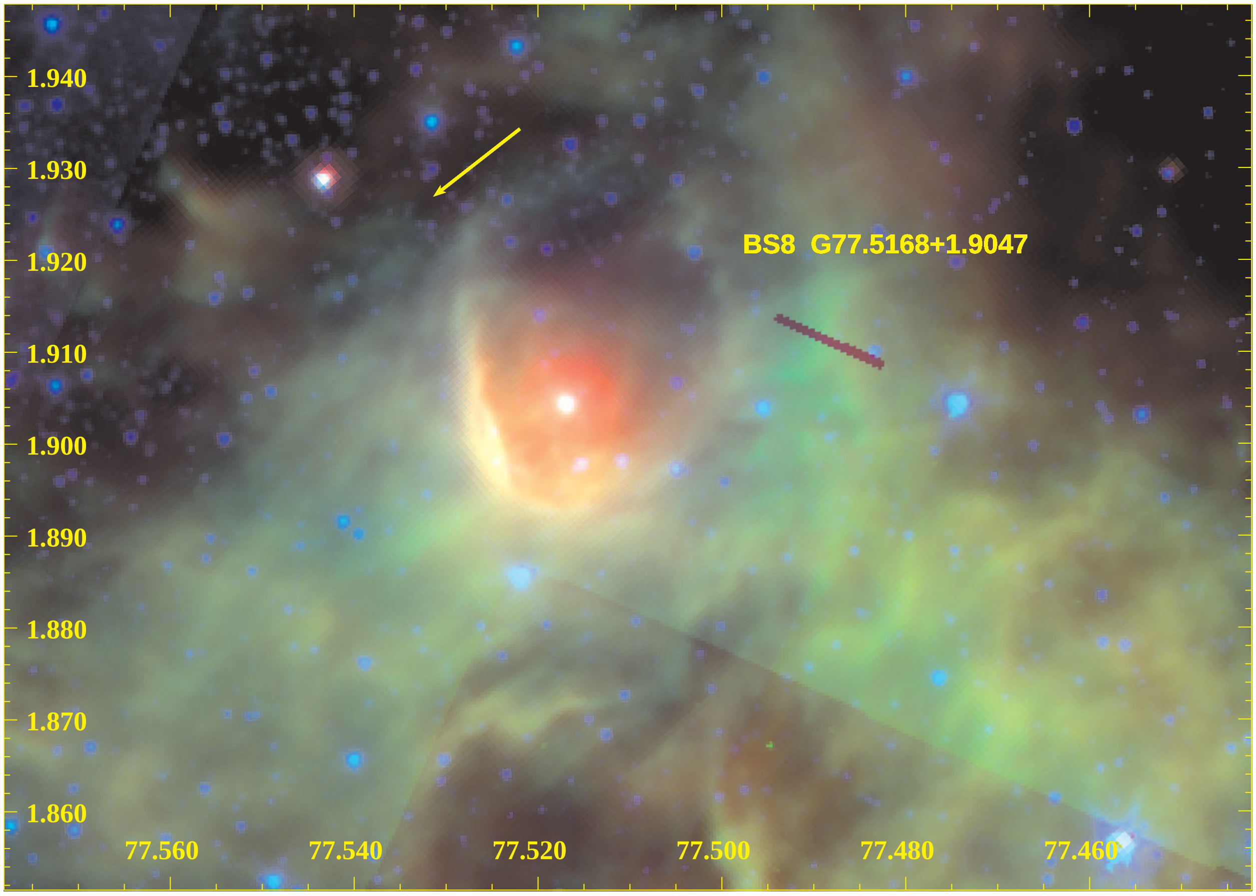

Fig. 9.— Three-color image of Bowshock Candidate 8, as in Figure 1.

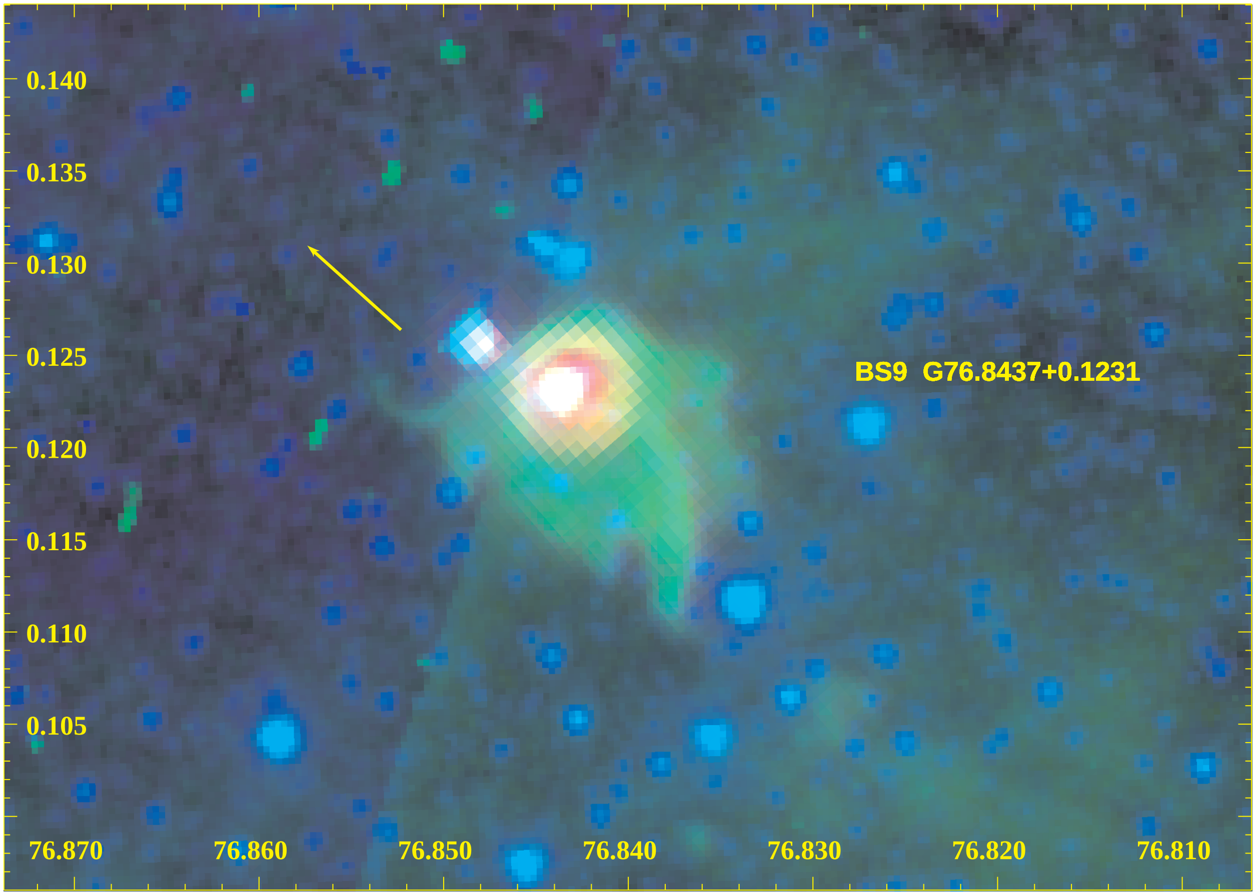

Fig. 10.— Three-color image of Bowshock Candidate 9, as in Figure 1.

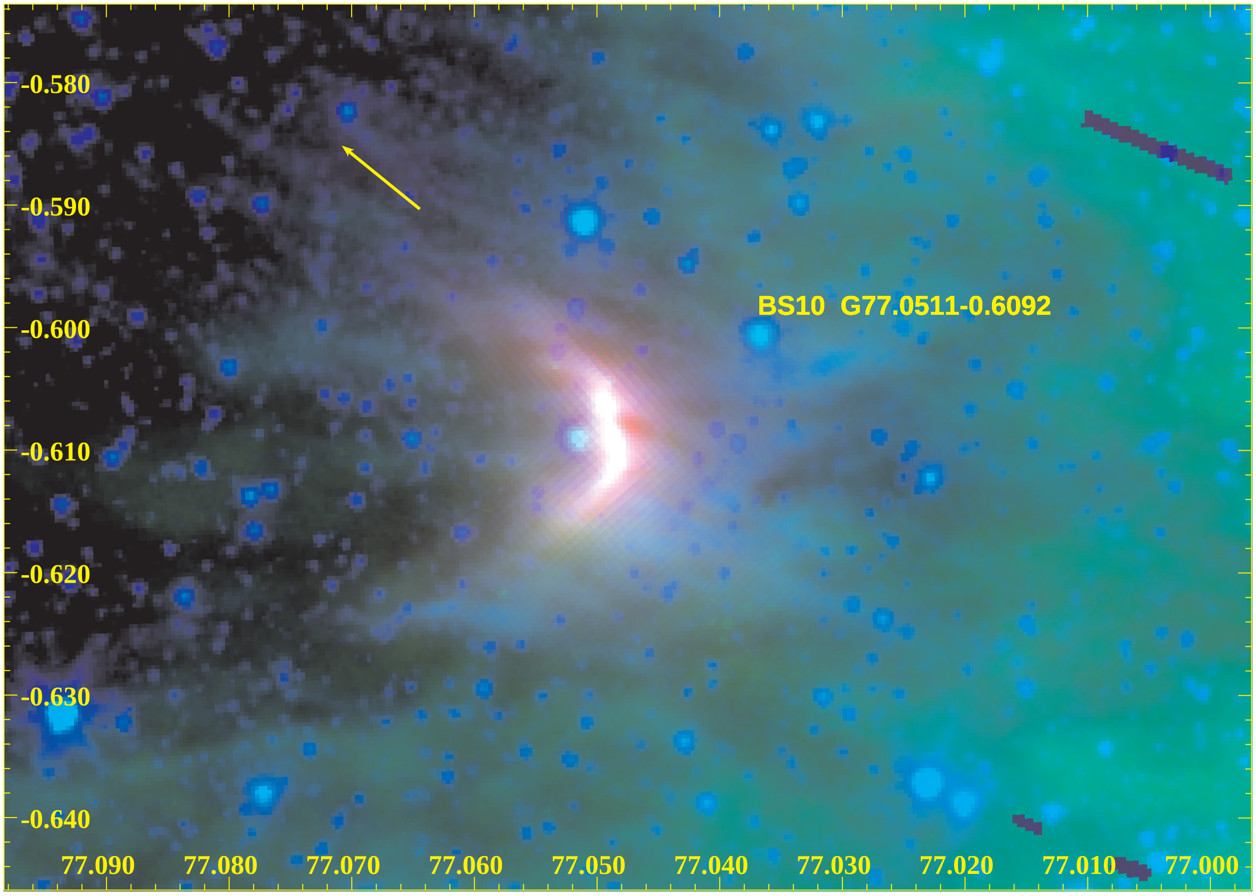

Fig. 11.— Three-color image of Bowshock Candidate 10, as in Figure 1.

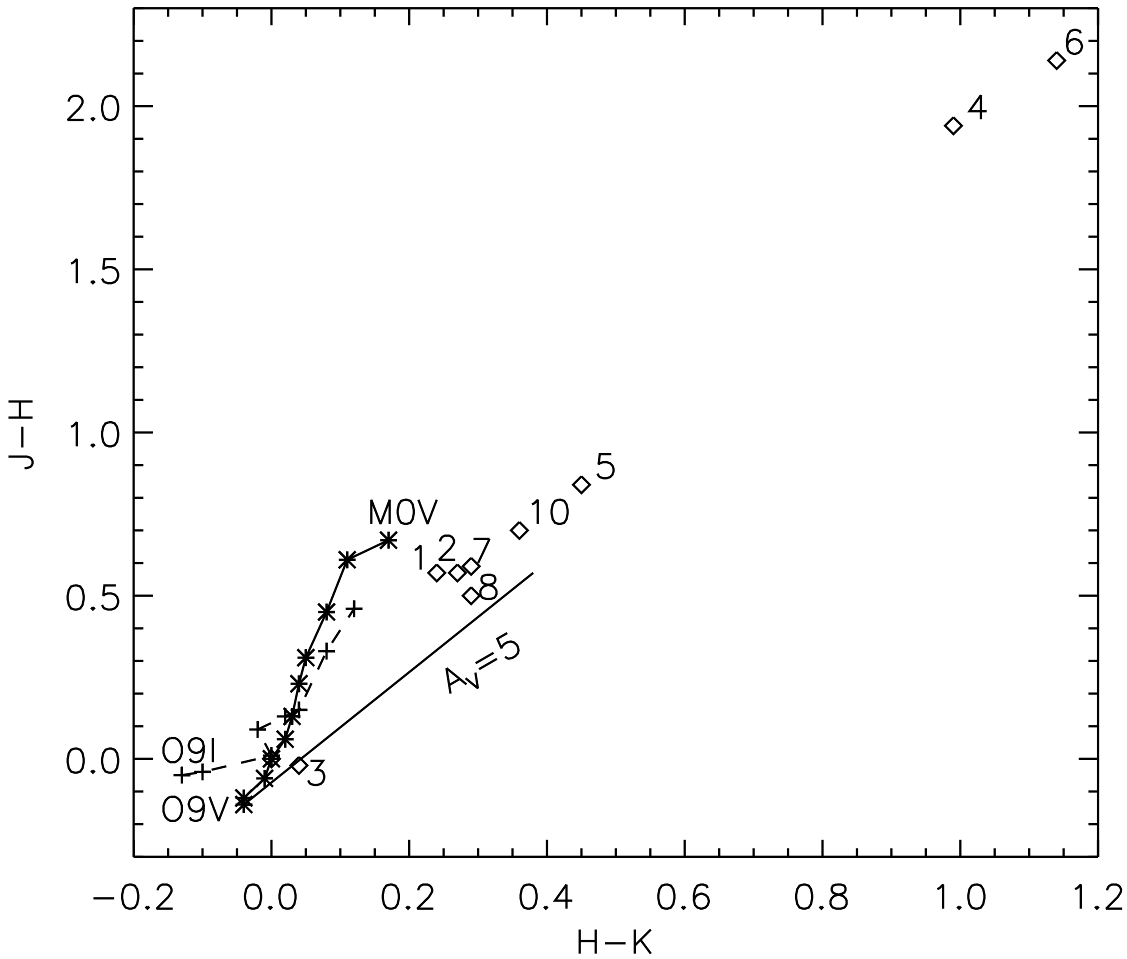

Fig. 12.— A JHK color-color diagram showing the sample stars (*diamonds*) in relation to the fiducial main sequence and supergiant sequence (*solid line* and *dashed line*). The reddening vector shows the equivalent of 5 magnitudes of visual extinction based on the Cardelli et al. (1989) reddening curve.

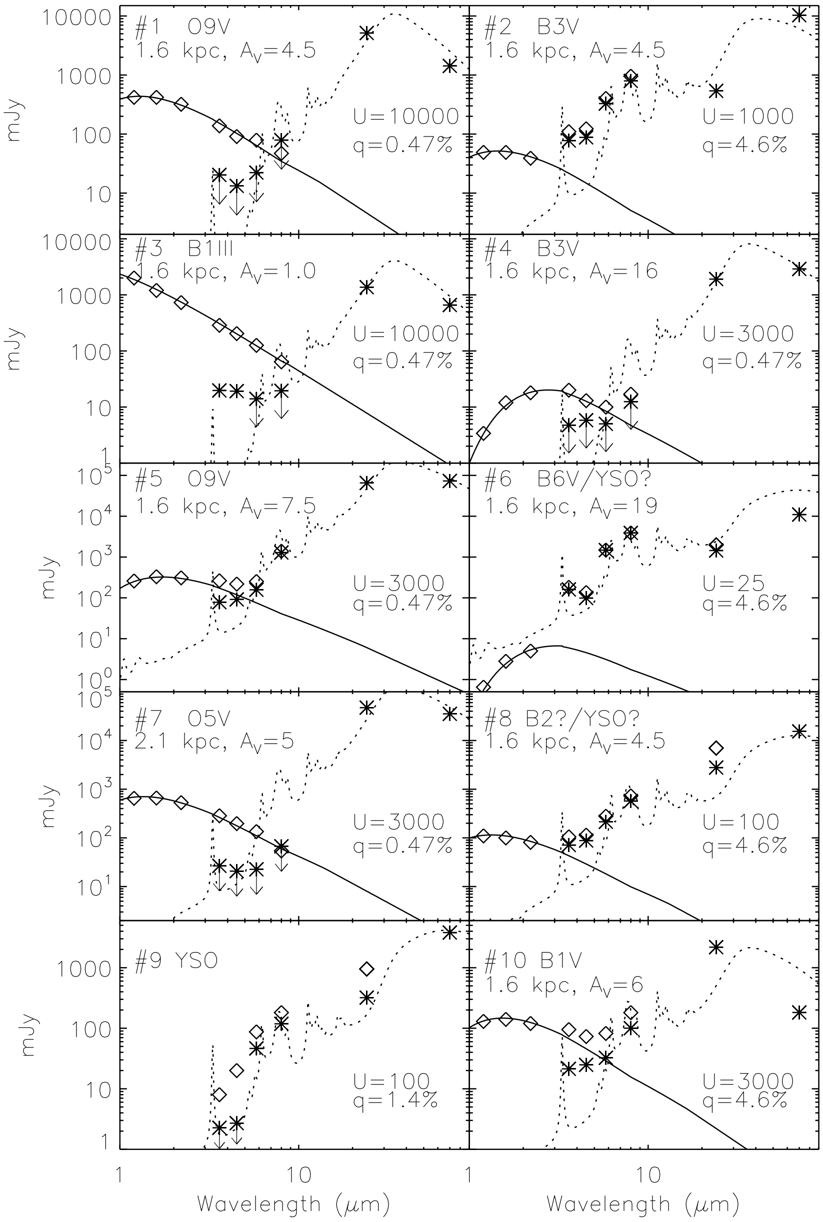

Fig. 13.— Infrared spectral energy distributions of the sample nebulae based on the photometry from Table 2.

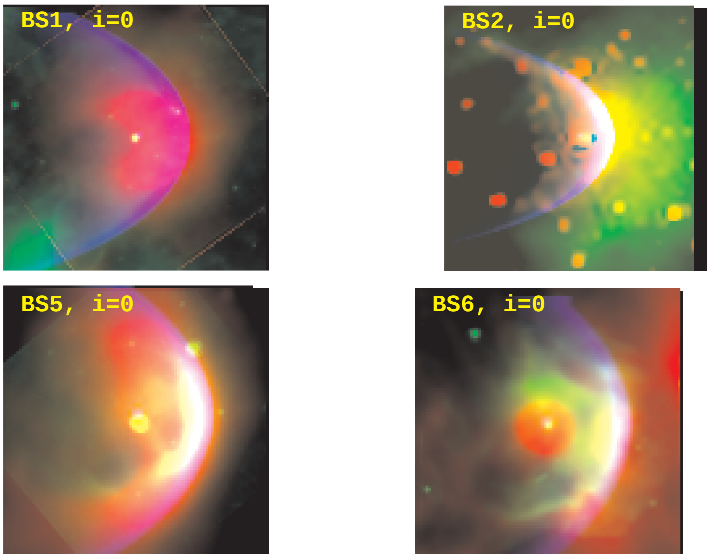

Fig. 14.— Images of selected bowshocks with [24] in red, [8.0] in green, and a simulated bowshock, based on the analytical shape parameterization of Wilkin (1996), in blue. The angular scales and rotations are arbitrarily adjusted to facilitate comparison between the data and models.

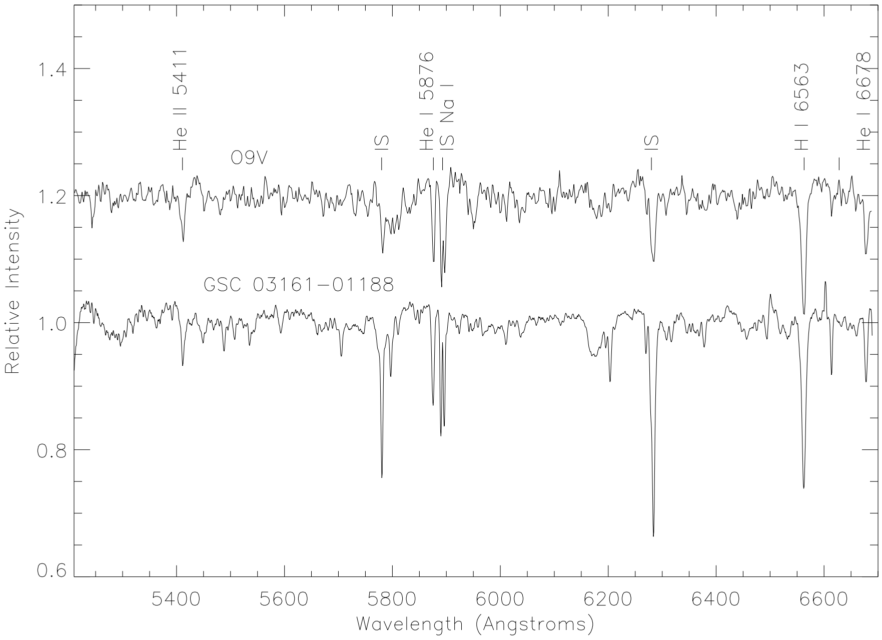

Fig. 15.— Standard O9V spectrum from Jacoby et al. (1984) (top) and WIRO spectrum of Star 1 (GSC03161-01188) (bottom). The relative strengths of the H I 6563 Å, He I 6678 Å and He II 5411 Å lines lead us to classify GSC03161-01188 as a O9V. IS denotes interstellar bands.

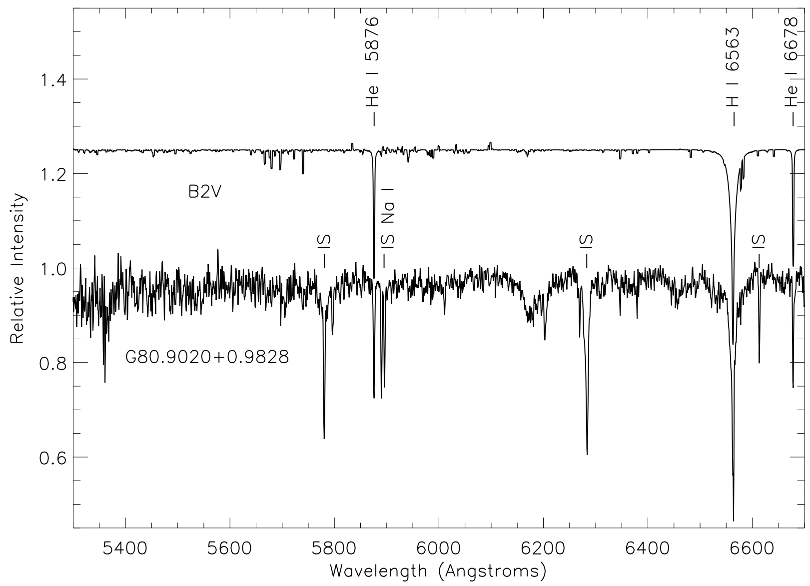

Fig. 16.— A model atmosphere B2V equivalent spectrum from Lanz & Hubeny (2003) (top) smoothed to the resolution of the data and WIRO spectrum of Star 2 (bottom). The relative strengths of the H I 6563 Åand the He I 6678 Å and He I 5876 Å lines lead us to classify this star as B2V, plus or minus two spectral subclasses. IS denotes interstellar bands.

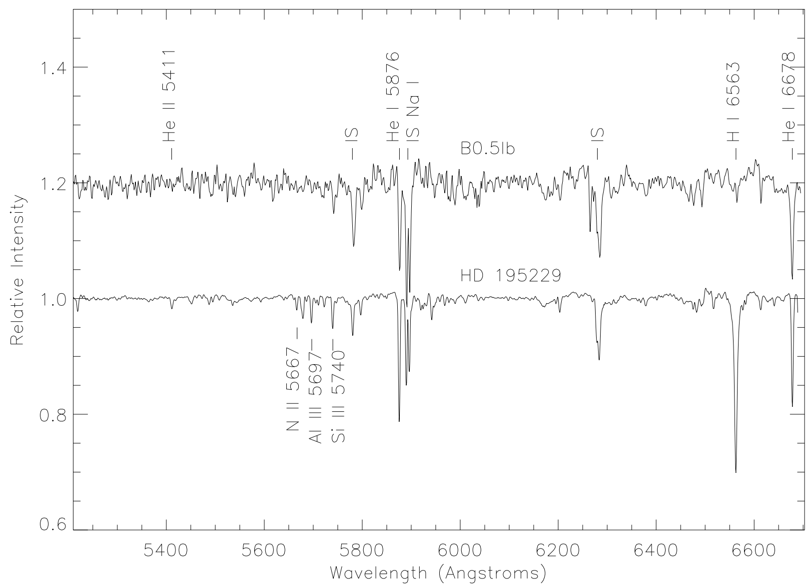

Fig. 17.— Standard B0.2III spectrum from Jacoby et al. (1984) (top) and WIRO spectrum of Star 3 (HD195229) (bottom). The WIYN spectrum of Star 3 in Figure 18 was used to determine this star's spectral type.

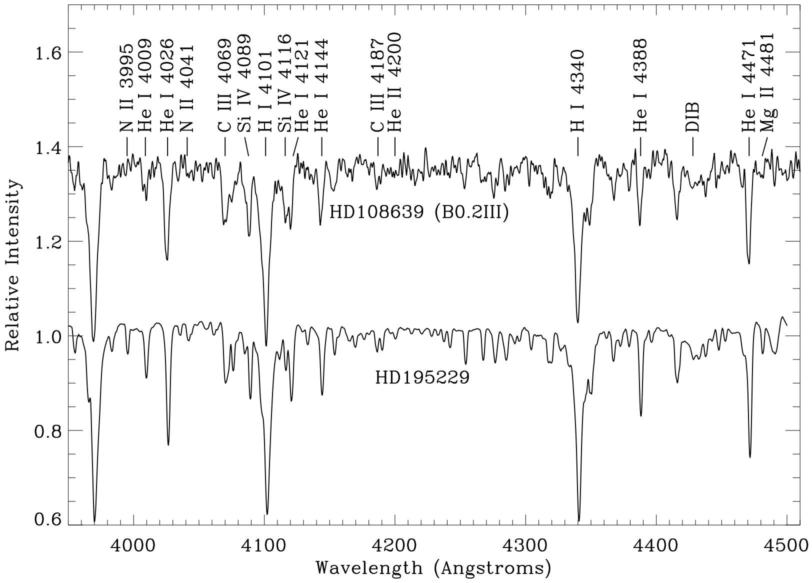

Fig. 18.— Standard B0.2III spectrum of HD108639 (Walborn & Fitzpatrick 1990) and WIYN spectrum of Star 3 (HD195229) (bottom). The strengths of the Si IV 4089, Si IV 4116 Å and C III 4069 Å lines identify the star as B0.2III.

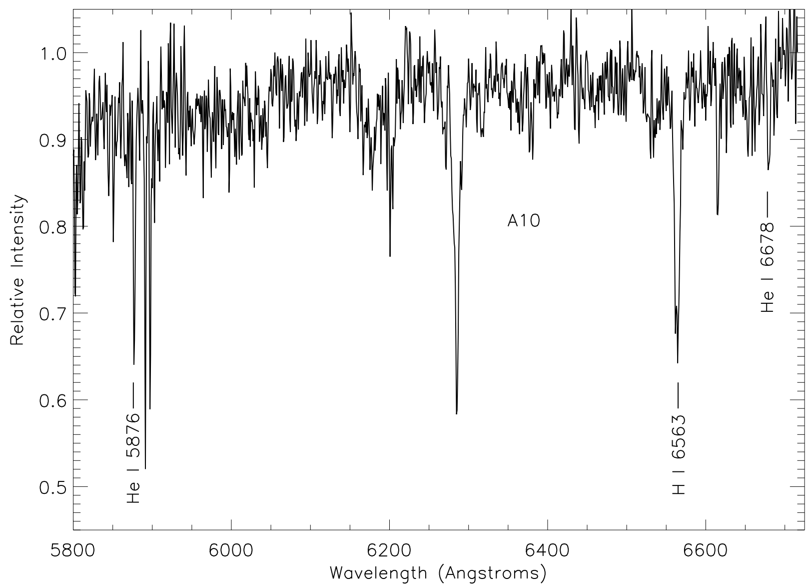

Fig. 19.— WIRO spectrum of Star 5, also known as A10 in the notation of Comerón et al. (2002). The spectrum is consistent with a late O star, although we estimate the uncertainty to be several spectral subclasses owing to the low signal-to-noise ratio of the spectrum.

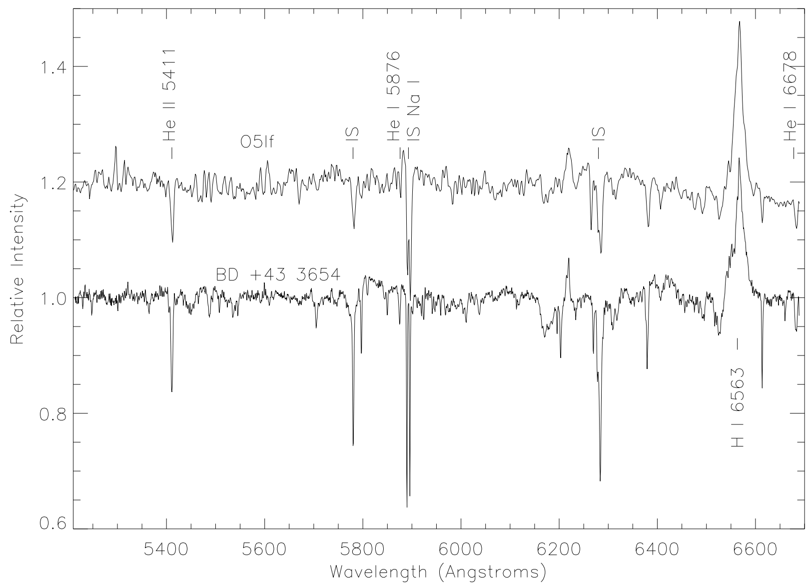

Fig. 20.— WIRO spectrum of BD+43°3654. Comparison with a standard O5If from Jacoby et al. (1984) (the earliest O supergiant in this library) agrees with the O4If classification given by Comerón & Pasquali (2007).